Glycobiology, 2023, **33**, 10, 784–800
https://doi.org/10.1093/glycob/cwad060
Advance access publication date 20 July 2023
Original Article

Contemporary human H3N2 influenza A viruses require a low threshold of suitable glycan receptors for efficient infection

Cindy M. Spruit[1], Igor R. Sweet[1], Joshua C.L. Maliepaard[2], Theo Bestebroer[3], Pascal Lexmond[3], Boning Qiu[4], Mirjam J.A. Damen[2], Ron A.M. Fouchier[3], Karli R. Reiding[2], Joost Snijder[2], Sander Herfst[3], Geert-Jan Boons[1,5], Robert P. de Vries[1,*]

[1]Department of Chemical Biology & Drug Discovery, Utrecht Institute for Pharmaceutical Sciences, Utrecht University, Universiteitsweg 99, 3584CG Utrecht, The Netherlands, [2]Biomolecular Mass Spectrometry and Proteomics, Bijvoet Center for Biomolecular Research and Utrecht Institute of Pharmaceutical Sciences, Utrecht University, Padualaan 8, 3584CH Utrecht, The Netherlands, [3]Department of Viroscience, Erasmus University Medical Center, Dr. Molewaterplein 50, 3015GE Rotterdam, The Netherlands, [4]Department of Pharmaceutics, Utrecht Institute for Pharmaceutical Sciences, Utrecht University, Universiteitsweg 99, 3584CG Utrecht, The Netherlands, [5]Complex Carbohydrate Research Center, University of Georgia, 315 Riverbend Rd, Athens, GA 30602, United States

*Corresponding author: Department of Chemical Biology & Drug Discovery, Utrecht Institute for Pharmaceutical Sciences, Utrecht University, Universiteitsweg 99, 3584CG Utrecht, The Netherlands. Email: r.vries@uu.nl

Recent human H3N2 influenza A viruses have evolved to employ elongated glycans terminating in α2,6-linked sialic acid as their receptors. These glycans are displayed in low abundancies by (humanized) Madin-Darby Canine Kidney cells, which are commonly employed to propagate influenza A virus, resulting in low or no viral propagation. Here, we examined whether the overexpression of the glycosyltransferases β-1,3-N-acetylglucosaminyltransferase and β-1,4-galactosyltransferase 1, which are responsible for the elongation of poly-N-acetyllactosamines (LacNAcs), would result in improved A/H3N2 propagation. Stable overexpression of β-1,3-N-acetylglucosaminyltransferase and β-1,4-galactosyltransferase 1 in Madin-Darby Canine Kidney and "humanized" Madin-Darby Canine Kidney cells was achieved by lentiviral integration and subsequent antibiotic selection and confirmed by qPCR and protein mass spectrometry experiments. Flow cytometry and glycan mass spectrometry experiments using the β-1,3-N-acetylglucosaminyltransferase and/or β-1,4-galactosyltransferase 1 knock-in cells demonstrated increased binding of viral hemagglutinins and the presence of a larger number of LacNAc repeating units, especially on "humanized" Madin-Darby Canine Kidney–β-1,3-N-acetylglucosaminyltransferase cells. An increase in the number of glycan receptors did, however, not result in a greater infection efficiency of recent human H3N2 viruses. Based on these results, we propose that H3N2 influenza A viruses require a low number of suitable glycan receptors to infect cells and that an increase in the glycan receptor display above this threshold does not result in improved infection efficiency.

Key words: sialic acid.; poly-LacNAc; influenza; H3N2; genetic glycoengineering.

Introduction

Influenza A viruses (IAV) of the H3N2 subtype cause seasonal epidemics, leading to illness, hospitalizations, and deaths in humans (Jester et al. 2020). The crucial first step of infection is the binding of the viral hemagglutinin (HA) to a receptor on a cell, which are glycans terminating in α2,6-linked sialic acids (Sia) for human IAVs (Rogers and Paulson 1983; Stevens et al. 2006). Because of continuous immune evasion, antigenic drift of the surface proteins of IAVs takes place. This antigenic drift of IAVs has changed receptor specificities (Yang et al. 2015) and pandemic H1N1 viruses (starting from 2009) were shown to prefer binding to glycans with multiple consecutive LacNAc repeating units (Canales et al. 2023). Furthermore, recent H3N2 viruses only bind to longer glycans having multiple consecutive *N*-acetyllactosamine (LacNAc) moieties terminating in an α2,6-linked Sia (Stevens et al. 2006, 2010; Chandrasekaran et al. 2008; Nycholat et al. 2012; Gulati et al. 2013; Yang et al. 2015; Peng et al. 2017; Sriwilaijaroen et al. 2018; Byrd-Leotis et al. 2019a). This specificity is most pronounced for H3N2 viruses of subclade 3C.2a, which require at least 3 subsequent LacNAc repeating units for binding (Broszeit et al. 2021).

These altered receptor specificities make it difficult to isolate and propagate H3N2 viruses, greatly hampering the further study of these viruses (Asaoka et al. 2006; Oh et al. 2008; Chambers et al. 2014; Peng et al. 2017; Takada et al. 2019). Even when virus isolation is successful, viruses may have acquired adaptive mutations in the receptor binding site of HA, especially when isolated in eggs instead of Madin-Darby Canine Kidney (MDCK) cells, which are often used for the propagation of IAV (Medeiros et al. 2001; Lee et al. 2013; Chambers et al. 2014; Allen and Ross 2018; Takada et al. 2019; Peck et al. 2021). MDCK cells have previously been modified to produce more α2,6-linked Sias by the overexpression of the enzyme ST6GAL1, resulting in MDCK-SIAT1 (Matrosovich et al. 2003) and MDCK-AX4 (Hatakeyama et al. 2005) cells. These cells enabled the isolation of H3N2 viruses, especially of the 3C.2a and 3C.3a subclades, and resulted in higher titers of viral stocks (Oh et al. 2008; Lin et al. 2017). To allow the isolation of further evolved

Received: February 16, 2023. **Revised:** July 3, 2023. **Accepted:** July 16, 2023
© The Author(s) 2023. Published by Oxford University Press. All rights reserved. For permissions, please e-mail: journals.permissions@oup.com
This is an Open Access article distributed under the terms of the Creative Commons Attribution Non-Commercial License (https://creativecommons.org/licenses/by-nc/4.0/), which permits non-commercial re-use, distribution, and reproduction in any medium, provided the original work is properly cited. For commercial re-use, please contact journals.permissions@oup.com

contemporary H3N2 viruses, with higher titers and fewer mutations, MDCK cells were further modified to eliminate α2,3-linked Sias while also overexpressing α2,6-linked Sias, resulting in "humanized" MDCK (hCK) cells (Takada et al. 2019).

Analysis of the *N*-glycans of MDCK, MDCK-SIAT1, and hCK cells indicated a low abundance of glycans with at least 3 successive LacNAc repeating units terminating in an α2, 6-linked Sia (Fig. S1; Byrd-Leotis et al. 2022). The enzyme β-1, 3-N-acetylglucosaminyltransferase (B3GNT2) is responsible for the addition of N-acetylglucosamine to glycans, whereas the galactose is transferred to the glycan by the enzyme β-1, 4-galactosyltransferase 1 (B4GALT1). Previously, we successfully used these 2 enzymes to elongate LacNAc repeating units both in chemoenzymatic synthesis (Li et al. 2019; Liu et al. 2019) and on biological membrane surfaces of erythrocytes (Broszeit et al. 2021).

We previously showed that the supplementation of Sia-depleted MDCK cells with *N*-glycans bearing 3 consecutive LacNAc repeating units is essential for infection of contemporary H3N2 viruses, as *N*-glycans with 1 or 2 LacNAc repeating units did not support infection (Peng et al. 2017). However, such an approach is not viable for many laboratories as the methods and means for glycolipid-engineering of cells are not widely available. Here, we genetically installed *N*-glycans having elongated LacNAc moieties on MDCK and hCK cells by the overexpression of B3GNT2 and B4GALT1, to obtain a cell line that can be used by many laboratories to study viral propagation. Surprisingly, although the B3GNT2/B4GALT1 knock-in cells exhibited elevated binding of recent H3 HAs, the overexpression did not lead to improved virus isolation and infection efficiency. Several studies have indicated that a higher display of appropriate receptors leads to increased infectivity (Matrosovich et al. 2003; Hatakeyama et al. 2005; Lin et al. 2012; Takada et al. 2019), whereas others indicated that only low amounts of receptors are required for infection (Kumari et al. 2007; Rimmelzwaan et al. 2007; Liu et al. 2022). Based on our studies, we concluded that above a required threshold, a greater number of suitable glycan receptors for H3N2 IAVs does not result in increased infection efficiency.

Results

Generation of stable B3GNT2 and B4GALT1 knock-in MDCK and hCK cell lines

Recently, we and others have shown that poly-LacNAc containing *N*-glycans are critical for the binding of contemporary H3N2 viruses and pandemic H1N1 viruses (Peng et al. 2017; Broszeit et al. 2021; Canales et al. 2023). Therefore, we used the glycosyltransferases B3GNT2 and B4GALT1 to increase the biosynthesis of LacNAc repeating units to produce extended *N*-glycans (Li et al. 2019; Liu et al. 2019; Wang et al. 2020; Broszeit et al. 2021). We hypothesized that the overexpression of B3GNT2 and/or B4GALT1 in MDCK and hCK cells would produce appropriate glycan receptors for recent H3N2 (subclade 3C.2a) IAVs.

To accomplish the overexpression of these genes in MDCK and hCK cells, lentiviral transfer plasmids encoding the human *B3GNT2* and/or *B4GALT1* genes, together with the *Hygromycin B resistance* gene, were constructed. The genes were expressed from 1 human EF-1α promoter (Wang et al. 2017) and separated by P2A (and for double glycosyltransferase knock-ins also T2A) self-cleaving peptides. Lentiviruses were produced with a transfer plasmid and packaging plasmids, after which the viruses were used to transduce MDCK and hCK cells (Fig. 1a). Cells in which the genes were inserted in the genome were selected with Hygromycin B.

Stable overexpression of *B3GNT2* and *B4GALT1* was confirmed by RT-qPCR analysis on isolated cellular RNA. Primers for the *B3GNT2*, *B4GALT1*, and *ST6GAL1* genes were used, and the obtained values were normalized to the reference gene *GAPDH* (Fig. 1b). Overexpression of the control gene *ST6GAL1* was clearly shown in hCK but not MDCK cells. Furthermore, the overexpression of *B3GNT2* and *B4GALT1* was present in all glycoengineered cell lines in which these knock-ins were made. It should be noted that expression levels in the double knock-in cell lines showed lower expression of the glycosyltransferases, especially for *B3GNT2* in MDCK-B3GNT2-B4GALT1 cells.

Thereafter, the protein levels of B3GNT2, B4GALT1, and ST6GAL1 in cell lysates were measured using proteomic experiments based on liquid chromatography coupled to tandem mass spectrometry (MS), using label-free quantitation relative to tubulin-β expression (Fig. 1c). Only peptides unique for the human B3GNT2, B4GALT1, and ST6GAL1 were selected. The proteomic data is comparable to the RT-qPCR data since elevated protein levels in the cell lines with knock-ins were observed. Collectively, the data showed that the stable overexpression of B3GNT2 and B4GALT1 in MDCK and hCK was successful.

Flow cytometric characterization of B3GNT2 and B4GALT1 knock-in cells with plant and viral lectins

Next attention was focused on whether the overexpression of B3GNT2 and/or B4GALT1 led to a display of a higher number of LacNAc repeating units on *N*-glycans. The glycans on the cell surface were first characterized using flow cytometry with standard lectins (Fig. 2b, specificities are summarized in Table SI). An alive, single-cell population was selected using a standard gating strategy, and mean fluorescence intensities were calculated over the cell population (Fig. 2a).

Sambucus nigra agglutinin (SNA; Shibuya et al. 1987) was used to detect α2,6-linked Sias, which are present in higher quantities on hCK cells than MDCK cells because of the overexpression of ST6GAL1 (Fig. 2b), which is consistent with earlier studies (Byrd-Leotis et al. 2022). The B3GNT2 and/or B4GALT1 knock-ins caused minimal (<2-fold) differences in α2,6-linked Sia display, which is understandable since we did not interfere with the sialyltransferases. *Lycopersicon esculentum* lectin (LEL) recognizes elongated glycans (Sweeney et al. 2018) and we observed that glycans capped with α2,6-linked Sias need at least 4 consecutive LacNAc repeating units to be recognized, whereas glycans capped with α2,3-linked Sias were recognized when presented on 2 successive LacNAc repeating units (Fig. S2), which explains the lower signal for all hCK cells in general. An ~2-fold increase in the binding of LEL to MDCK-B4GALT1 and MDCK-B3GNT2-B4GALT1 compared with wild-type (WT) MDCK cells was observed, indicating that the LacNAc repeating units on MDCK cells are indeed elongated by the overexpression of mainly B4GALT1. Moreover, we observed an increase in LEL signal in the hCK-B3GNT2 cells compared with the hCK WT cells, indicating that the overexpression of B3GNT2 resulted in the formation of longer glycans on hCK cells. *Erythrina crista-galli* lectin

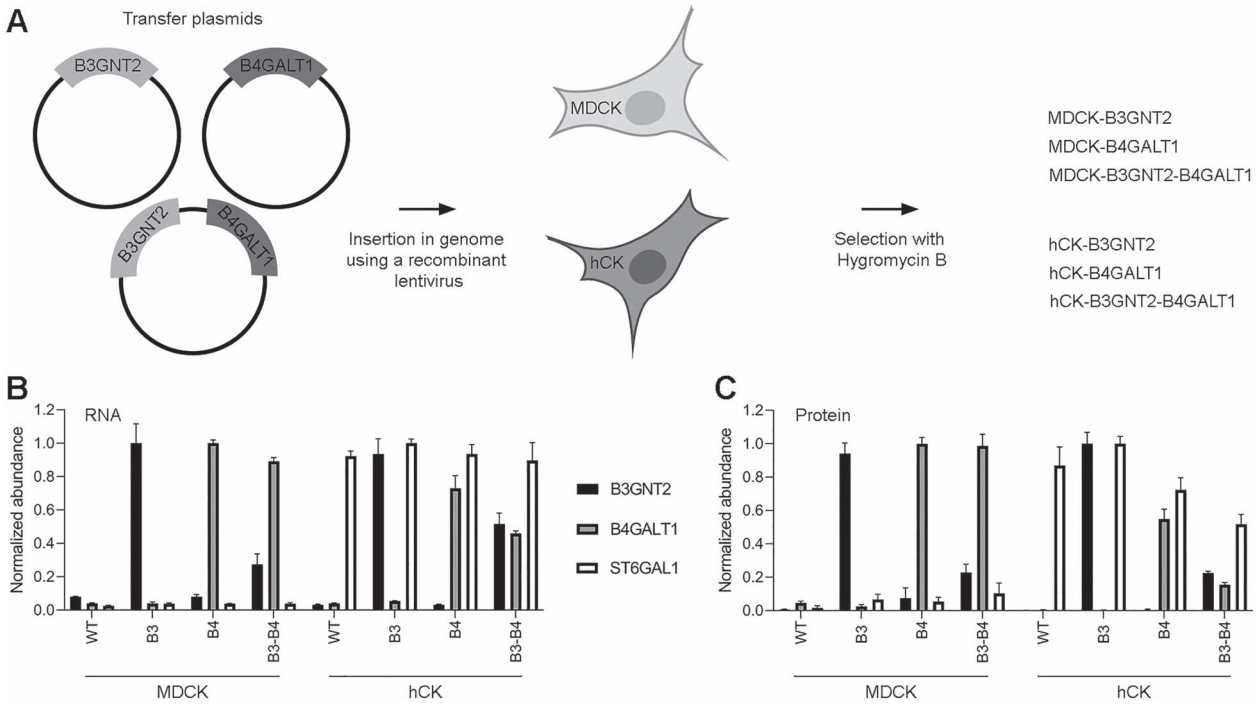

Fig. 1. Construction of MDCK and hCK cells that overexpress B3GNT2 and/or B4GALT1. a) MDCK and hCK cells were modified with recombinant lentiviruses containing transfer plasmids for the insertion of the *B3GNT2* and/or *B4GALT1* gene and the Hygromycin B resistance gene. The knock-in cells were selected with 300 μg/ml Hygromycin B. b) RT-qPCR was performed with primers that anneal to both the human and dog *B3GNT2, B4GALT1,* or *ST6GAL1* genes. The values relative to the dog *GAPDH* gene were used, which were then normalized to the highest value of each gene. Mean and SD (n = 3) are shown. c) Peptide MS of the B3GNT2, B4GALT1, and ST6GAL1 proteins. Only peptides unique to human proteins were selected. All samples were normalized against tubulin-β and then normalized to the highest value of each protein. Mean and SD (n = 3) are shown.

(ECA) recognizes terminal galactose, and thus glycans lacking Sia capping (Broszeit et al. 2019). The results using ECA indicated that all MDCK cells have a larger proportion of non-sialylated glycans compared with all hCK cells, which agrees with the overexpression of ST6GAL1 in all hCK cells. No major differences of more than 2-fold in the amount of non-sialylated glycans between WT and B3GNT2 and/or B4GALT1 knock-in cells were observed.

In addition to commonly employed plant lectins, viral proteins were used to examine the glycans displayed on the cells (Fig. 2b, specificities are summarized in Table SI). The N-terminal domain of γCoV/AvCoV/guinea fowl/France/14032/2014 (Gf-CoV-2014 NTD) is known to bind elongated glycans (Bouwman et al. 2019). MDCK-B4GALT1 and MDCK-B3GNT2-B4GALT1 cells showed an increased Gf-CoV-2014 NTD signal compared with MDCK WT cells. Furthermore, hCK WT cells appeared to have a higher number of LacNAc repeating units on glycans than MDCK WT cells. The hCK-B3GNT2 cells, and the hCK-B4GALT1 and hCK-B3GNT2-B4GALT1 cells to a lesser extent, showed a substantial increase (at least 2-fold) in Gf-CoV-2014 NTD binding compared with the hCK WT cells, indicating the presence of additional LacNAc repeating units on glycans. The HA of A/Vietnam/1203/2004 H5N1 is commonly used to probe the presence of terminal α2,3-linked Sias (Broszeit et al. 2019; Spruit et al. 2021, 2022). We observed a much lower amount of α2,3-linked Sias in all hCK cells compared with all MDCK cells, which is in agreement with the knock-outs of all β-galactoside α-2,3 sialyltransferases that were made in the hCK cells previously (Takada et al. 2019) and findings in earlier studies (Byrd-Leotis et al. 2022). The B3GNT2/B4GALT1 knock-ins did not alter the α2,3-linked Sia content. The HA of the human IAV A/Puerto-Rico/8/1934 H1N1 (PR8) H1 binds α2,6-linked Sias (Nemanichvili et al. 2019) and showed increased binding to all hCK cells compared with all MDCK cells, which is related to the overexpression of ST6GAL1 in hCK cells (Takada et al. 2019). Increased binding of PR8 to MDCK-B4GALT1 and MDCK-B3GNT2-B4GALT1 compared with MDCK WT cells was also observed, which is more pronounced than the results obtained with SNA.

hCK-B3GNT2 cells are preferentially bound by contemporary H3 HAs

After initial characterization, an array of human H3 HAs was used for flow cytometric binding studies with B3GNT2 and B4GALT1 knock-in cells (Fig. 2c, specificities are summarized in Table SI). To cover a broad scope of receptor binding specificities, HAs from viruses from different years (1968–2019) and (sub)clades were chosen. Three HAs from the 3C.2a subclade (A/Singapore/INFH-16-0019/2016, A/Netherlands/00010/2019, and A/Hong-Kong/4801/2014) were chosen to assess the presence of glycans with elongated LacNAc structures (Broszeit et al. 2021) on the MDCK and hCK WT and B3GNT2/B4GALT1 knock-in cells.

These human H3 HAs prefer binding to terminal α2,6-linked Sias over terminal α2,3-linked Sias and therefore, in general, more binding is observed to hCK WT cells than to MDCK WT cells. The HA of A/Hong-Kong/1/1968 does not require multiple consecutive LacNAc repeating units for binding, but it does show a strong preference for glycans with 3 or 4 consecutive LacNAc repeating units compared with glycans with only 1 or 2 repeating units (Peng et al. 2017). The preference of the HA of A/Hong-Kong/1/1968 for

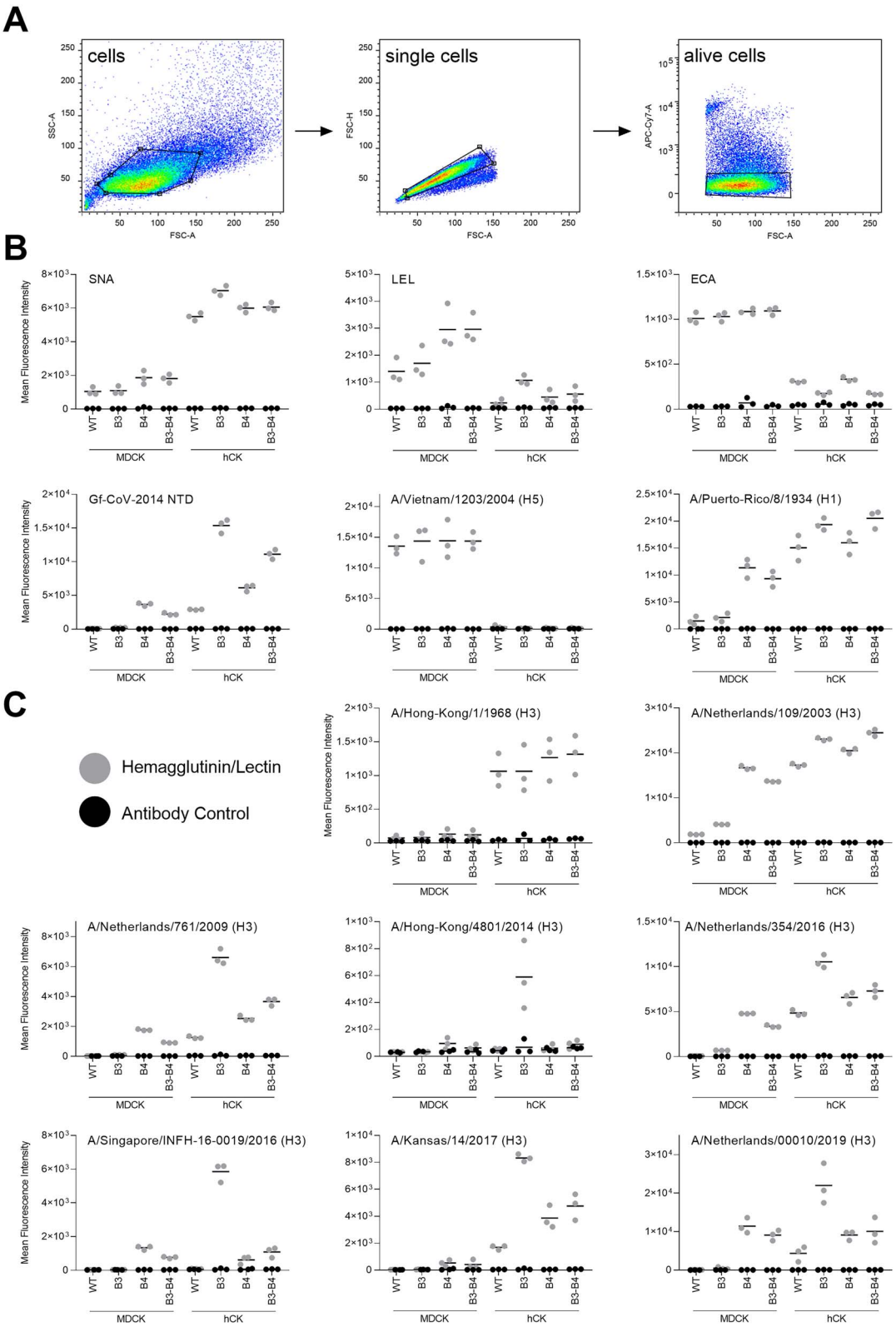

Fig. 2. Flow cytometric characterization of B3GNT2/B4GALT1 knock-in MDCK and hCK cells. a) The gating strategy that was used to select single, alive cells. b) Flow cytometry measurements with lectins SNA (recognizes α2,6-Sia), LEL (recognizes elongated glycans), and ECA (recognizes glycans without Sia) were performed. Furthermore, Gf-CoV-2014 NTD was used to detect elongated glycans, H5 HA of A/Vietnam/1203/2004 was used to detect α2,3-Sia, and H1 HA from A/Puerto-Rico/8/1934 was used as a standard influenza virus. Triplicate measurements were performed, of which the mean and all individual measurements are displayed. c) A diverse set of H3 HAs was used to characterize the cells. Triplicate measurements were performed, of which the mean and all individual measurements are displayed. Titration curves of A/Hong-Kong/1/1968, A/Netherlands/109/2003, and A/Singapore/INFH-16-0019/2016 are shown in Fig. S4. Flow cytometric experiments with neuraminidase treatment of the cells are shown in Fig. S3.

longer glycans is, however, not observed in our flow cytometry experiments, since the B3GNT2 and B4GALT1 knock-in cells did not show increased binding.

The human H3N2 IAVs A/Netherlands/109/2003 and A/Netherlands/761/2009 were previously shown to bind terminal α2,6-linked Sias presented on glycans with both 2 and 3, but not 1, consecutive LacNAc repeating units (Broszeit et al. 2021). Increased binding of at least a 2-fold difference of the HA of A/Netherlands/109/2003 to all MDCK knock-in cells and all hCK cells compared with MDCK WT cells was observed. Similar binding patterns were observed for the HA of A/Netherlands/761/2009, although the binding to hCK-B3GNT2 cells was much more pronounced and no increased binding to MDCK-B3GNT2 cells was observed. Interestingly, the MDCK-B4GALT1 and MDCK-B3GNT2-B4GALT1 cells often showed comparable or higher binding to the recent H3 HAs than the hCK WT cells, whereas low levels of α2,6-linked Sias are present on all MDCK cells.

As described in the introduction, contemporary H3 IAVs are known to bind to terminal α2,6-linked Sias presented on glycans with multiple consecutive LacNAc repeating units, which is especially true for H3N2 viruses of subclade 3C.2a that require at least 3 subsequent LacNAc repeating units for binding. Increased binding to MDCK-B4GALT1, MDCK-B3GNT2-B4GALT1, and all hCK cell lines compared with MDCK WT cells was observed for the recent H3 HAs (2014–2019) A/Netherlands/354/2016, A/Singapore/INFH-16-0019/2016 (subclade 3C.2a), A/Kansas/14/2017 (subclade 3C.3a), and A/Netherlands/00010/2019 (subclade 3C.2a). The hCK-B3GNT2 cells that were already indicated to have the longest glycans by LEL and Gf-CoV-2014 NTD, also showed a substantial increase in binding of these recent H3 HAs compared with all other cell lines investigated. The strong binding to hCK-B3GNT2 cells of the HA of A/Hong-Kong/4801/2014 (subclade 3C.2a) was even more obvious, as other cell lines appeared to be barely bound to this HA.

Lectin binding to cells is concentration and Sia-dependent

To investigate whether the binding of the H3 HAs in the flow cytometry experiments was indeed specific for Sias, we performed experiments with neuraminidase-treated cells (Fig. S3). As controls for the removal of α2,3-linked or α2,6-linked Sias, the H5 HA of A/Vietnam/1203/2004 (Broszeit et al. 2019; Spruit et al. 2021, 2022) and SNA (Shibuya et al. 1987) were used. These lectins showed a decrease in the binding signal after neuraminidase treatment. When testing 2 H3 HAs with well-defined binding specificities, A/Netherlands/109/2003 and A/Netherlands/761/2009 (Broszeit et al. 2021), decreases in binding after neuraminidase treatment were also obtained, indicating that the binding of H3 HAs was indeed Sia-dependent.

When examining the binding of the HAs of human H3N2 viruses to cells in Fig. 2c, there appeared to be no binding to the MDCK WT cells at all for A/Hong-Kong/1/1968, A/Netherlands/761/2009, A/Hong-Kong/4801/2014, A/Netherlands/354/2016, A/Singapore/INFH-16-0019/2016, A/Kansas/14/2017, and A/Netherlands/00010/2019, even though it is possible to propagate these viruses in MDCK WT cells. To investigate whether binding to MDCK cells occurred at all, a titration with H3 HAs was performed. As a positive control, A/Netherlands/109/2003 was used since binding was observed in Fig. 2c. Furthermore, the HAs of the well-defined A/Hong-Kong/1/1968 (Peng et al. 2017) and the subclade 3C.2a virus A/Singapore/INFH-16-0019/2016 were used. The titration (Fig. S4) indicated that there is indeed binding to MDCK WT cells of these HAs but to a much lesser extent than to hCK WT (or hCK-B3GNT2 cells). From the flow cytometric experiments, it appeared that the hCK-B3GNT2 cells present the highest number of consecutive LacNAc repeating units compared with the other cell lines investigated.

Elongated N-glycans are detected on hCK-B3GNT2 cells

Since *N*-glycans are the most relevant receptors on cells for IAV (Chu and Whittaker 2004), we further investigated the *N*-glycans of WT and B3GNT2/B4GALT1 knock-in MDCK and hCK by HILIC-IMS-QTOF positive mode MS of released *N*-glycans. Compared with MDCK WT cells, all 7 other cell lines showed a large reduction in the relative abundance of high-mannose glycans (Fig. S5a), to which IAV does not bind. Possibly, the presence of high-mannose glycans is influenced by the overexpression of other glycosyltransferases (Hossler et al. 2007; Ren et al. 2019), changes in glycan processing time or enzyme spatial localization (Hossler et al. 2007), or a combination of multiple factors (Mastrangeli et al. 2020). This increase in the relative abundance of complex and hybrid *N*-glycans may partially explain the improved binding phenotype of the H3 HAs to cell lines different than MDCK WT as observed in the flow cytometry experiments (Fig. 2c).

From the flow cytometry experiments, the hCK-B3GNT2 cells were expected to have the highest number of LacNAc repeating units compared with the other 7 cell lines (Fig. 2c). The data obtained from the *N*-glycan HILIC-IMS-QTOF positive mode MS experiments indeed showed a higher relative abundance of *N*-glycans with more than 3 LacNAc repeating units in hCK-B3GNT2 compared with hCK WT cells (Fig. 3a). The HILIC-IMS-QTOF positive mode MS data on the *N*-glycans with at least 1 LacNAc repeating unit were further analyzed to determine the relative abundance of glycans with a different number of LacNAc repeating units in the 8 different cell lines (Fig. 3b). Overall, relatively less glycans were detected with 4 or more LacNAc repeating units compared with an earlier study on MDCK and hCK WT cells (Byrd-Leotis et al. 2022), of which the meta-analysis is presented in Fig. S1a, although different methods were used in the previous study and not all peaks were assigned. Most importantly, the highest increase in the relative abundance of elongated *N*-glycans was observed in hCK-B3GNT2 cells (Fig. 3b), which agrees with the flow cytometric results (Fig. 2b and c).

For binding of contemporary H3N2 IAVs, *N*-glycans with at least 3 consecutive LacNAc repeating units should be capped with α2,6-linked Sias. While we were unable to determine the Sia linkage, we analyzed the percentage of sialylation of the *N*-glycans with at least 1 LacNAc repeating unit (Fig. S5b). In general, 75–96% of these *N*-glycans were sialylated, except for the glycans of MDCK-B3GNT2 cells (38% sialylated), which correlated with the low binding of H3 HAs as observed using flow cytometry (Fig. 2c). Notably, meta-analysis of a previous study (Byrd-Leotis et al. 2022) showed even lower degrees of sialylation of glycans from MDCK and hCK WT cells (65 and 79%, respectively, Fig. S1b), although the methods used in this study were different. Whereas non-sialylated *N*-glycans occurred in all groups of LacNAc lengths in MDCK WT and B3GNT2/B4GALT1 knock-in cells, all *N*-glycans with at least 4 LacNAc repeating units (except

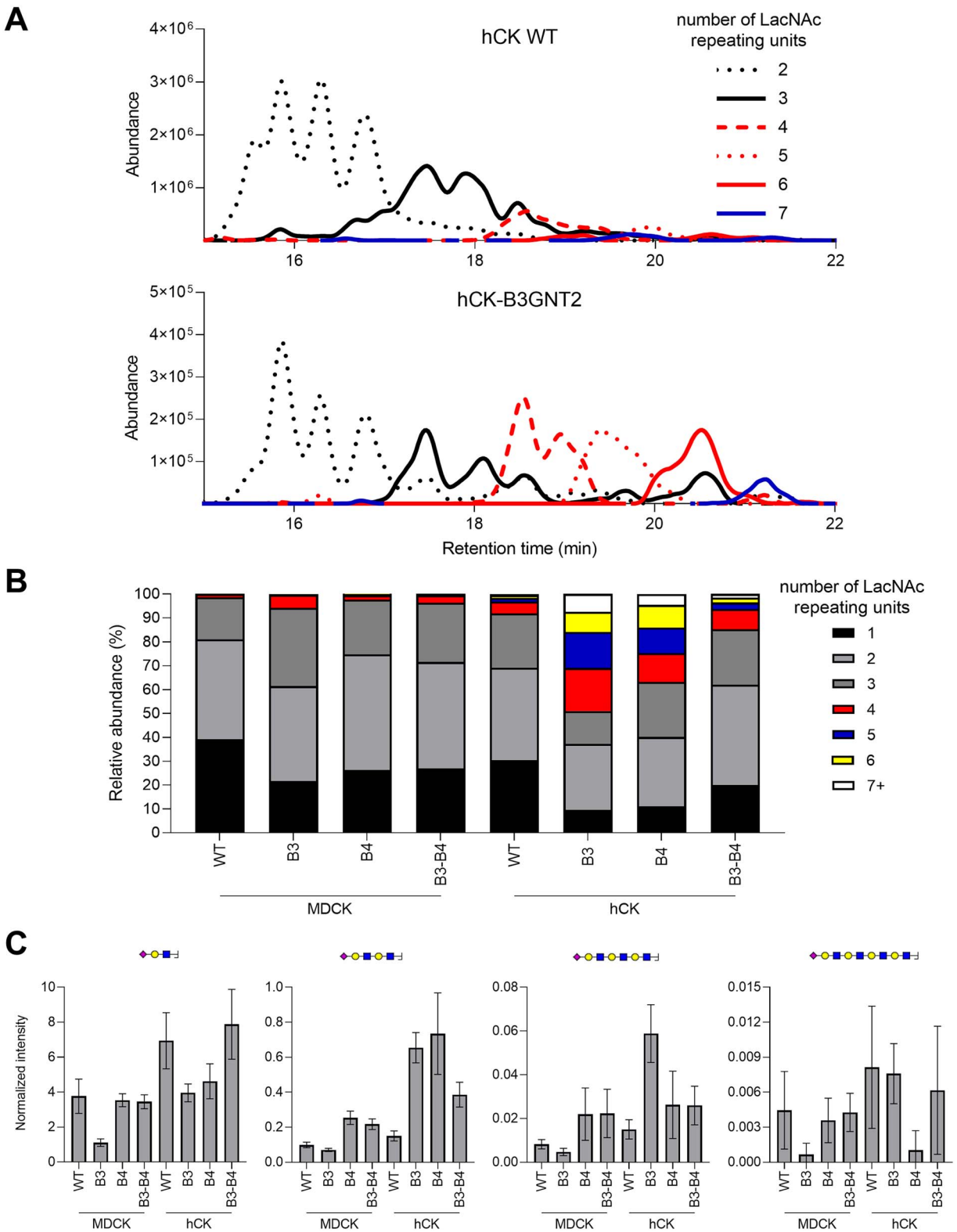

Fig. 3. *N*-glycan analysis of WT and B3GNT2/B4GALT1 knock-in MDCK and hCK cells using MS. The *N*-glycans from WT and B3GNT2/B4GALT1 knock-in MDCK and hCK cells were measured using HILIC-IMS-QTOF positive mode MS. a) Chromatograms of hCK WT and hCK-B3GNT2 cells were constructed for the glycans with at least 2 and at most 7 LacNAc repeating units. The extracted-ion-counts for the 10 most abundant glycan features per LacNAc repeating unit group were summed to yield a chromatogram. b) The *N*-glycans found in HILIC-IMS-QTOF positive mode MS with at least 1 LacNAc repeating unit were analyzed for the number of LacNAc repeating units present and the relative abundance was calculated. Further analysis is presented in Fig. S5. Full glycan feature lists for each cell line are presented in Tables SII–SIX. c) Analysis of the *N*-glycans was additionally performed by LC–MS/MS, followed by analysis of the glycan oxonium ions (Table SX). Sia capped (repeating) LacNAc oxonium ions with masses (from left to right) 657.2349, 1,022.3671, 1,387.4993, and 1,752.6315 were identified and the amounts detected were normalized to the core fragments. Mean and standard errors (n = 3) are shown. Further analysis is shown in Fig. S6 and annotated spectra are present in Fig. S7.

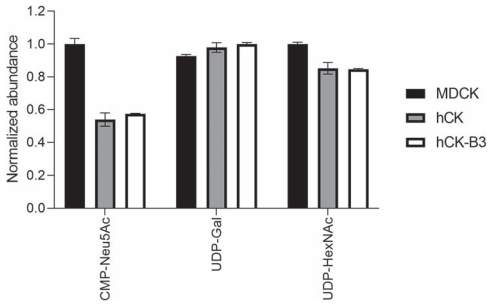

Fig. 4. Sugar nucleotide analysis of MDCK, hCK, and hCK-B3GNT2 cells. The sugar nucleotides in the lysate of MDCK, hCK, and hCK-B3GNT2 cells were analyzed by MS ($n = 2$). The normalized abundance of CMP-Neu5Ac, UDP-Gal, and UDP-HexNAc are shown. Normalization was performed on the cell line with the highest amount of each sugar nucleotide. Detailed information about all measured sugar nucleotides is presented in Fig. S8.

for 4 glycans in total) on all hCK cell lines were sialylated (Tables SII–SIX).

To further elucidate the *N*-glycan structures, MS/MS experiments were performed. As outcome, we integrated from MS/MS spectra the relative abundance of oxonium ions that could indicate glycan structural elements (Table SX). These included, among others, LacNAc repeating units from 1 to 4 units (respectively, *m/z* 366.1395, 731.2717, 1,096.4039, and 1,461.5361), as well as their variants with *N*-acetylneuraminic acid (NeuAc) sialylation (respectively, *m/z* 657.2349, 1,022.3671, 1,387.4993, and 1,752.6315). While included in the analysis, no 2-keto-3-deoxynonic acid, *N*-glycolylneuraminic acid (NeuGc), acetylation, sulfation, or phosphorylation were found. On the other hand, several ions were detected that could delineate α-Gal and bisection, although these were low in intensity and could overlap with other compositions. We focused on the glycan fragments with 1–4 consecutive LacNAc repeating units, both with and without Sia (Figs 3c, S6, and S7), since contemporary H3N2 IAV require at least 3 consecutive LacNAc repeating units for binding.

Although the knock-in cell lines MDCK-B4GALT1 and MDCK-B3GNT2-B4GALT1 did not show an increase in the number of LacNAc repeating units compared with MDCK WT in MS1 analysis (Fig. 3b), a clear increase in the glycan fragments with 2 and 3 consecutive LacNAc repeating units was observed compared with MDCK WT cells (Figs 3c and S6). In MDCK-B3GNT2 and hCK WT cells, the relative increase of glycans with 4 LacNAc repeating units in the MS1 analysis was a few percent compared with MDCK WT cells (Fig. 3b). However, for the MDCK-B3GNT2 cells, this relative increase in consecutive LacNAc repeating units is not observed (Figs 3c and S6). For the hCK WT cells, the MS1 and MS/MS analyses correlate, since a slight increase in the sialylated glycan fragments with 1–4 consecutive LacNAc repeating units (Fig. 3c) was observed. In contrast, in an earlier study (Byrd-Leotis et al. 2022), slightly more glycans with 4 or more LacNAc repeating units were found to be present on MDCK WT cells compared with hCK WT cells (meta-analysis presented in Fig. S1a). The relative abundance of LacNac repeating units in our MS1 analysis was even higher in hCK-B3GNT2-B4GALT1 cells (Fig. 3b), which is also observed in the MS/MS analysis when looking at the sialylated glycan fragments with 2 and 3 LacNAc repeating units (Fig. 3c).

Surprisingly, hCK-B4GALT1 showed a substantial increase in the relative abundance of *N*-glycans with a higher number of LacNAc repeating units compared with hCK WT cells in the MS1 analysis, up to even 9 LacNAcs (Fig. 3b and Table SVIII), which was not expected from the results of the flow cytometry experiments (Fig. 2). The high relative abundance of LacNAc repeating units in hCK-B4GALT1 cells (Fig. 3b) appears to be presented mainly as sialylated fragments with 2 instead of 3 or 4 consecutive LacNAc repeating units (Fig. 3c), which explains the lower binding of H3 HAs to these cells compared with hCK-B3GNT2 cells in the flow cytometry experiments (Fig. 2c). Most sialylated glycan fragments with 3 consecutive LacNAc repeating units, the required receptor for contemporary H3N2 IAV, were found on hCK-B3GNT2 (Fig. 3c), which again correlates to the increased binding of H3 HAs as observed in flow cytometry (Fig. 2c).

Sugar nucleotides are not a limiting factor in the biosynthesis of poly-LacNAc structures

Changes in sugar nucleotide levels have been observed in cells after overexpression of B3GNT2 and B4GALT1 (Wang et al. 2020). Although a clear increase in the number of consecutive LacNAc repeating units was observed in especially hCK-B3GNT2 cells, we wondered whether the further elongation of glycans may have been limited by depletion of sugar nucleotides. Therefore, the concentrations of sugar nucleotides in the cell lysates of MDCK WT, hCK WT, and hCK-B3GNT2 cells were measured by MS (Fig. 4, with details in Fig. S8; van Scherpenzeel et al. 2022). The overexpression of ST6GAL1 in hCK WT and hCK-B3GNT2 cells compared with MDCK WT cells resulted in elevated levels of sialylation and thereby lower levels of available CMP-Neu5Ac, which was also demonstrated in the sugar nucleotide analysis. No other major differences or depletions of sugar nucleotides were observed in any of the cell lines. Most importantly, the sugar nucleotides that are required for the biosynthesis of LacNAc repeating units (UDP-galactose and UDP-HexNAc) were not depleted in any of the cell lines, thus sugar nucleotide availability is likely not a limiting factor for the elongation of glycans.

Improved binding of HAs to cells does not ensure higher virus titers and improved isolation of influenza viruses

MDCK WT, hCK WT, and B3GNT2 and/or B4GALT1 knock-in cells were inoculated with H3N2 viruses to investigate whether higher titers could be obtained in the knock-in cells. Four control viruses (H3N2 from 2003, H1N1, and influenza B, Fig. 5a) and 8 recent (2017–2019) H3N2 viruses from the 3C.2a (Fig. 5b) and 3C.3a (Fig. 5c) subclades were used for inoculation. For the H3N2 virus from 2003, the H1N1 virus, and the influenza B viruses, no substantial difference was observed between the virus titers obtained in MDCK, hCK, or B3GNT2/B4GALT1 knock-in cells (Fig. 5a).

Recent 3C.2a viruses are known to only bind glycans having at least 3 consecutive LacNAc repeating units, whereas recent 3C.3a viruses also bind glycans with 2 consecutive LacNAc repeating units (Broszeit et al. 2021). For the 3C.2a viruses, a considerable difference was visible between the titers in MDCK WT and hCK WT cells (Fig. 5b), which correlates with the increased binding as observed in the flow cytometric experiments (Fig. 2). Surprisingly, no substantial difference

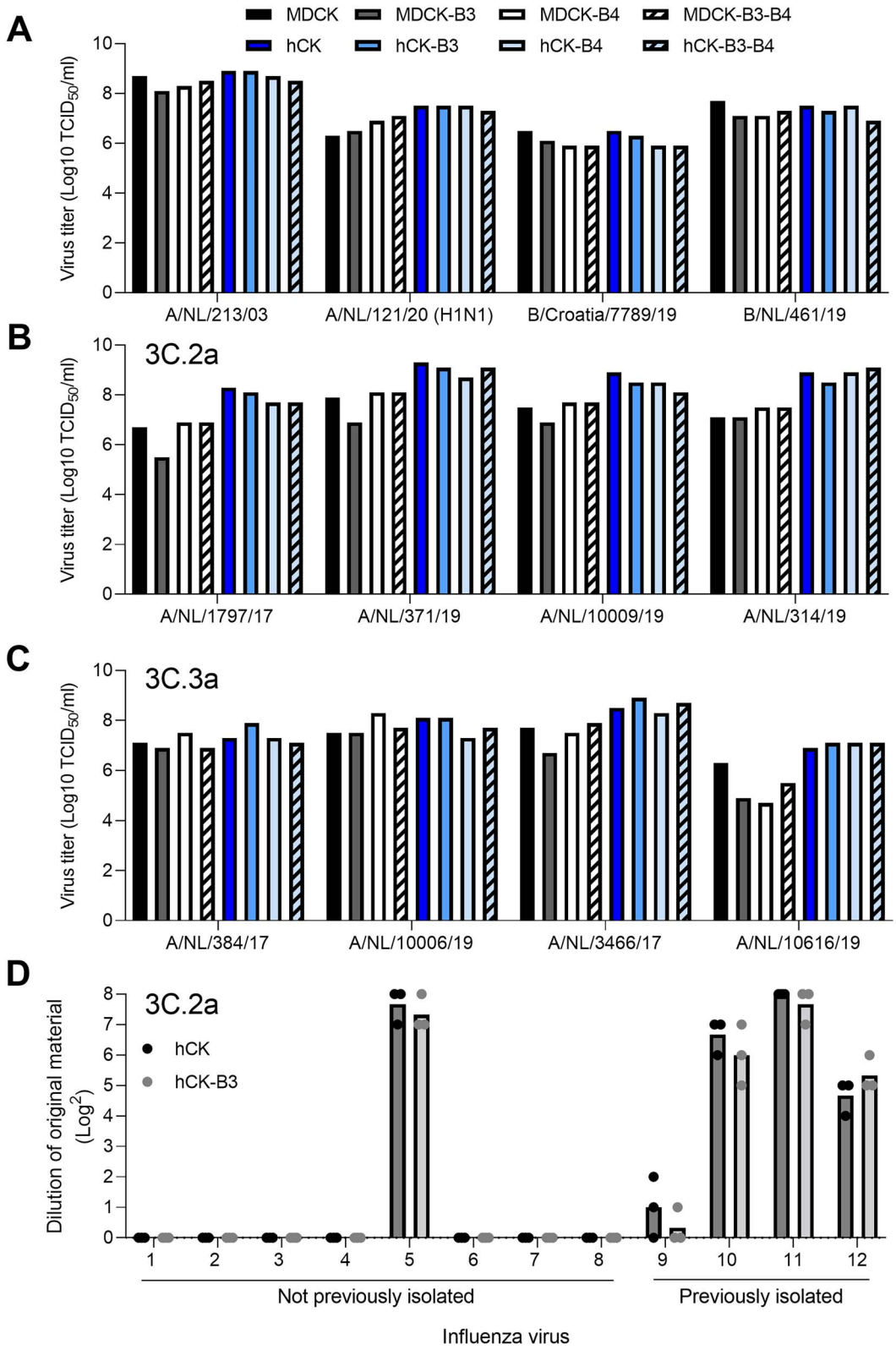

Fig. 5. Influenza virus inoculation of B3GNT2 and B4GALT1 knock-in MDCK and hCK cells. End-point titrations with 4 control viruses and 8 recent H3N2 IAVs (details in Table 1) were performed, of which a) 4 control viruses, b) 4 3C.2a viruses, and c) 4 3C.3a viruses. Infectious titers were determined either using a hemagglutination assay a) or a NP staining b, c) when a hemagglutination assay was not possible. d) An infection study using hCK and hCK-B3GNT2 cells with a 2-fold dilution of 12 H3N2 IAVs from the 3C.2a clade (details in Table 2) that could previously either not be isolated in hCK cells (#1–8) or could be isolated in hCK cells (#9–12) was performed. Infection was assessed by the presence of cytopathic effects. Individual and mean values are shown.

between the titers in hCK WT and hCK-B3GNT2 cells was observed, whereas the glycans on the latter cell line were extended as observed in the flow cytometry (Fig. 2) and glycan MS experiments (Fig. 3). Furthermore, no difference was observed in the titers for the 3C.3a viruses (Fig. 5c), not even between MDCK and hCK cells. Therefore, we concluded that additional binding does not necessarily lead to a higher infection efficiency.

While additional strains of H3N2 viruses can be isolated in hCK cells as compared with MDCK-SIAT1 and MDCK cells (Takada et al. 2019), we noticed that some H3N2 viruses could still not be isolated in hCK cells. To investigate whether cell lines with longer glycans (hCK-B3GNT2 cells) would facilitate the isolation of additional virus strains, we attempted to isolate 12 H3N2 viruses (clade 3C.2a) from original patient material in hCK and hCK-B3GNT2 cells (Fig. 5d). Since hCK cells are better suited for the isolation of these viruses (Takada et al. 2019) and the original patient material was only available in limited quantities, we did not attempt to also isolate the viruses from MDCK cells. Eight of the tested viruses could not be isolated previously since they did not replicate in hCK cells (Fig. 5d). All viruses that were previously isolated in hCK cells were again successfully isolated. However, the use of hCK-B3GNT2 cells did not result in more efficient isolation of those viruses. Of the viruses that could not be isolated previously, only A/Netherlands/173/2019 could now be isolated. However, isolation was achieved in both hCK and hCK-B3GNT2 cells. Therefore, a higher number of extended glycans did not improve the isolation of H3N2 IAVs from the 3C.2a clade.

Discussion

Although we elongated the LacNAc repeating units on the glycans of MDCK and hCK cells, it did not result in a higher infection efficiency of recent H3N2 IAVs. It has been reported that a low but critical threshold of high-affinity receptors is required for infection (Kumari et al. 2007; Rimmelzwaan et al. 2007), though binding and infection are further assisted by the presence of high-abundance low-affinity receptors (Liu et al. 2022). We previously showed that the presence of high-affinity receptors is indeed essential for infection of cells (Peng et al. 2017). This implies that increased HA binding will lead to enhanced entry efficiency. It is therefore counterintuitive that presenting preferred ligands in copious amounts does not lead to increased infection. Strikingly, here we demonstrated that increased HA binding to cells does not necessarily result in more efficient infection.

On the other hand, several studies have indicated that increasing the number of preferred receptors will increase the infection efficiency of IAVs (Matrosovich et al. 2003; Hatakeyama et al. 2005; Lin et al. 2012; Takada et al. 2019), which was also shown with MDCK-SIAT1 (Matrosovich et al. 2003), MDCK-AX4 (Hatakeyama et al. 2005), and hCK (Takada et al. 2019) cells. A possible explanation for this discrepancy may lie in the glycoproteins on which *N*-glycans, the presumed glycan receptors for IAVs (Chu and Whittaker 2004), are presented. It has been suggested previously that only specific sialylated glycoproteins can be used as a receptor for IAV (Chu and Whittaker 2004; Karakus et al. 2020), such as the voltage-dependent Ca^{2+} channel $Ca_v1.2$ (Fujioka et al. 2018), NKp44 (Arnon et al. 2004; Ho et al. 2008), NKp46 (Mandelboim et al. 2001; Arnon et al. 2004; Achdout et al. 2010), epidermal growth factor (Eierhoff et al. 2010), and nucleolin (Chan et al. 2016). Although we demonstrated that glycans on B3GNT2/B4GALT1 knock-in cells contained a higher number of LacNAc repeating units, we have not determined on which glycoproteins the elongated glycans are present. Possibly, the glycans that are used as a receptor and are present on specific glycoproteins can be modified in their Sia linkage, as done in MDCK-SIAT1, MDCK-AX4, and hCK cells, but not in the number of LacNAc repeating units. Additionally, the glycoproteins on which the glycans are presented may not be clustered enough (Sieben et al. 2020) to support IAV infection. This would explain why the infection efficiency could not be increased by the elongation of LacNAc repeating units on MDCK and hCK cells.

Nevertheless, not all recent H3N2 IAVs could be isolated efficiently in hCK cells (Takada et al. 2019), as also shown in Fig. 5d. Possibly, no viable virus particles were present in the patient samples from which we attempted to isolate virus. Alternatively, we may be overlooking an identified (Mandelboim et al. 2001; Arnon et al. 2004; Ho et al. 2008; Achdout et al. 2010; Eierhoff et al. 2010; Chan et al. 2016; Fujioka et al. 2018) or an unidentified glycoprotein that is not present (in high enough quantities) on hCK cells. Furthermore, other types of glycans, such as phosphorylated (Byrd-Leotis et al. 2019b) and sulfated glycans (Gambaryan et al. 2005; Stevens et al. 2006, 2010), possibly act as a receptor for IAV. Because of our sample preparation for the released glycan MS analysis (acidic and basic conditions), we were unable to measure phosphorylated glycans. Potentially, some sulfated glycans could be partially retained. However, we did not detect sulfated glycans in the MS/MS analysis. To increase the isolation of recent H3N2 IAVs, it is of foremost importance to investigate the limiting factor in the infection efficiency of these viruses.

The overexpression of B3GNT2 and/or B4GALT1 is responsible for the elongation of glycans. Previously, overexpression of B4GALT1 was found to result in the elongation of glycans on CHO cells (Wang et al. 2020). From the flow cytometry analysis, B4GALT1 appeared to be the limiting factor for the elongation of glycans in MDCK cells, whereas the elongation was limited in hCK cells when B3GNT2 was not present in high enough amounts. Surprisingly, the elongation of glycans appeared to be inhibited in MDCK cells by the overexpression of B3GNT2, as can be observed when comparing MDCK-B3GNT2 cells with MDCK WT cells, but also when comparing MDCK-B3GNT2-B4GALT1 cells with MDCK-B4GALT1 cells. In the latter 2, the overexpression of B4GALT1 is at the same level (Fig. 1c), but longer glycans are present on MDCK-B4GALT1 cells (Figs 2b and c and 3c). In hCK cells, sialyltransferase expression is severely modified by the overexpression of ST6GAL1 and the knockout of all ST3GAL enzymes. Both the heavily overexpressed ST6GAL1 and B3GNT2 in hCK cells use terminal galactose as a substrate. The overexpression of B3GNT2 in hCK cells perhaps restores the balance between ST6GAL1 and B3GNT2, thereby allowing B3GNT2 to use the terminal galactose as a substrate again for the elongation of glycans before sialylation takes place. On the other hand, in MDCK cells, the balance may be skewed even more by the overexpression of B3GNT2, leading to the low sialylation of glycans on these cells (Fig. S5b). Furthermore, the cellular localization of the enzymes and potential enzyme complex

formation may be of importance, which is not regulated with overexpression alone.

Our observations indicate that only few suitable glycan receptors are required for efficient infection. This is in line with our previous observations that an increase from 2.7 to 8.7% of sialylated glycans with at least 3 consecutive LacNAc repeating units on, respectively, unmodified and modified turkey erythrocytes allowed for the binding of contemporary H3N2 viruses (Broszeit et al. 2021). Also in ferrets, an animal model that is often used to study human influenza viruses (Spruit et al. 2021), the presence of glycans in the respiratory tract (lung, trachea, soft palate, nasal turbinate, and nasal wash) was investigated. Elongated glycans were present solely as *N*-glycans, with a maximum of 9 LacNAc repeating units per glycan, but at most 0.17% of the detected glycans had at least 3 consecutive LacNAc repeating units terminating with Sia, which is required for H3N2 IAV binding (Jia et al. 2014). Although the glycans in the human trachea have not been analyzed yet, data are available on other parts of the human airway system. Sensitive methods indicated the presence of extended *N*-glycans with up to 10 LacNAc repeating units in human lung tissue. However, at most 0.3% of the *N*-glycans were found to contain at least 3 consecutive LacNAc repeating units. The *N*-glycans in the bronchus and nasopharynx contained a lower number of LacNAc repeating units than in the lung (Walther et al. 2013). Another study found *N*-glycans with up to 22 LacNAc repeating units in the lung. Even though the majority of the Sias were found to be α2,6-linked instead of α2,3-linked, the α2,6-linked Sias were mainly present on the shorter glycans (Jia et al. 2020), further supporting our conclusions that only minor amounts of suitable glycan receptors are required for efficient infection by IAVs. Therefore, we conclude that factors other than glycosylation must be investigated to address the suboptimal propagation of recent human H3N2 IAVs as an aid to their further study.

Material and methods

Cell culturing and preparation of cell lysates

Cells were cultured in DMEM (Gibco) with 10% FCS (S7524, Sigma) and 1% penicillin and streptomycin (Sigma). All hCK cells (Takada et al. 2019), knock-in and WT, were maintained with an additional 10 μg/ml blasticidin and 2 μg/ml puromycin in the medium. B3GNT2 and B4GALT1 knock-in cells were maintained in medium containing an additional 300 μg/ml Hygromycin B, a concentration that was determined to kill MDCK (CCL-34) and hCK (a kind gift from Yoshihiro Kawaoka) without Hygromycin B resistance genes. Detaching of the (knock-in) MDCK and hCK cells was always done using 1X TrypLE Express Enzyme (12605010, Thermo Fisher Scientific), using 2 ml in a T75 flask, at a confluency of ~90%.

Cell lysates were obtained after first washing cell monolayers once using D-PBS (D5837, Sigma). Cells were subsequently harvested after incubation at 37°C for 20 min with 1X TrypLE Express Enzyme (2 ml in a T75 flask) at a confluency of ~90%. The cell suspension was centrifuged for 5 min at 250 rcf. The cell pellets were lysed by the addition of RIPA lysis buffer (20–188, Merck Millipore) supplemented with protease inhibitor (A32965, Thermo Fisher Scientific), which was vortexed for 20 s. The suspension was incubated on ice for 30 min, after which it was centrifuged at 16,500 rcf in a fixed-angle centrifuge at 4°C, after which the supernatant was used as cell lysate.

Cloning of lentiviral transfer plasmids

Plasmid pCF525-EF1a-Hygro-P2A-mCherry-lenti (Watters et al. 2018) was a gift from Jennifer Doudna (Addgene plasmid # 115796) and was used as the backbone for the transfer plasmid. Three transfer plasmids were constructed (pCF-B3GNT2, pCF-B4GALT1, and pCF-B3GNT2-B4GALT1). The region between the P2A and WPRE was removed and replaced by either the *B3GNT2* or *B4GALT1*. When the genes of both glycosyltransferases were cloned into the plasmid they were connected with a T2A self-cleaving peptide. The *B3GNT2* and *B4GALT1* genes were always proceeded by the signal sequence of the human GalT, which we copied from the EGFP-GalT plasmid (gift from Jennifer Lippincott-Schwartz, Addgene plasmid # 11929; Cole et al. 1996). The T2A self-cleaving peptide was amplified from plasmid tetO.Sox9.Puro (Canals et al. 2018), which was a gift from Henrik Ahlenius (Addgene plasmid # 117269). The *B3GNT2* and *B4GALT1* genes were amplified from plasmids B3GNT2-pGEn2-DES and B4GALT1-pGEn2-DES, which are a gift from Kelly Moremen and are available via. All segments were amplified with an overhang, using the primers indicated in Table SXI. Assembly of the plasmids was performed using Gibson assembly, after which they were sequenced to ensure correct amplification and assembly.

Lentiviral integration of the *B3GNT2* and *B4GALT1* genes

Lentiviral particles were produced using HEK293T cells (Qiu et al. 2021). One of the transfer plasmids as described above, together with the packaging plasmids pMDLg/pRRE, pRSV-Rev, and pMD2.G, which were kind gifts from Didier Trono (Dull et al. 1998; Addgene plasmids #12251, #12253, and #12259, respectively) were used. The day before transduction, MDCK (CCL-34) and hCK cells were seeded in a 6-wells plate at a density of 100,000 cells per well. Transduction with 0.5–3 μl of lentivirus was performed in the presence of 8 μg/ml polybrene with 1 ml fresh medium per well. The medium was replaced with fresh medium containing 300 μg/ml Hygromycin B at 18 h after transduction. Cells were grown until no Hygromycin B sensitive cells were remaining. Cells were always maintained in the presence of 300 μg/ml Hygromycin B.

RT-qPCR analysis on *B3GNT2*, *B4GALT1*, and *ST6GAL1* genes

RNA extraction was performed using the GeneJET RNA purification kit (Thermo Fisher Scientific) according to the manufacturer's protocol, after which the DNA was treated with DNAse I (#EN0251, Thermo Fisher Scientific). RT-qPCR was performed using the Luna universal 1-step RT-qPCR kit (#E3005, New England Biolabs) according to the provided protocol, in which 10 ng of DNAse I-treated RNA was used. Primers (Table SXII) for *B3GNT2*, *B4GALT1*, and *ST6GAL1* were designed to anneal both in the human and dog genome. Primers for GAPDH (household/reference gene) were designed using the dog genome. Experiments were performed in triplicate and Ct values of the RT-qPCR experiments on the glycosyltransferases were compared with the average Ct value of GAPDH of that specific cell line under the assumption

that the amount of DNA doubles every cycle. The means and standard deviations of the amount of DNA relative to GAPDH were calculated.

Overexpression of B3GNT2, B4GALT1, and ST6GAL1 on the protein level

Cell lysates, obtained as described above, were further used for the label-free quantification of B3GNT2, B4GALT1, and ST6GAL1 proteins. From the cell lysates, 10 μg of protein was denatured, reduced, and alkylated by adding 100 μl of a solution consisting of 150 mM Tris, 5 mM tris(2-carboxyethyl)phosphine, 30 mM chloroacetamide, and 1% sodium deoxycholate (SDC) at pH 8.5. Next, 100 ng lysyl endopeptidase (129-02541, Wako Chemicals GmbH) and 100 ng trypsin (T1426, Sigma) were added and the samples were incubated overnight at 37°C. The samples were then acidified by adding formic acid (FA) to a concentration of 0.5% before solid-phase extraction (SPE) sample clean-up, causing the SDC to precipitate. SPE clean-up was performed on an Oasis HBL u-elution plate.

After the SPE clean-up, the samples were dried with a vacuum centrifuge. Subsequently, the sample was reconstituted in 2% FA before analysis on the Orbitrap Exploris mass spectrometer (Thermo Scientific) connected to a UHPLC 3000 system (Thermo). Approximately 200 ng of reconstituted peptides were trapped on a pre-column and then separated on a 50 cm × 75 μm Poroshell EC-C18 analytical column (2.7 μm) temperature controlled at 40°C. Solvent A consisted of 0.1% FA, solvent B of 0.1% FA in 80% acetonitrile, and different combinations of solvents A and B were used in the next steps. Trapping was performed for 1 min in 100% solvent A. Peptides were separated by a 65 min gradient of 9–44% buffer B followed by 44–99% B in 3 min, and 99% B for 4 min. MS data were obtained in a data-dependent acquisition mode. The full scans were acquired in the *m/z* range of 350–1,600 at the resolution of 60,000 (*m/z* 400) with AGC target 3E6. The most intense precursor ions were automatically selected for higher-energy collisional dissociation (HCD) fragmentation performed at normalized collision energy (NCE) 28, after accumulation to the target value of 1E5. MS/MS acquisition was performed at a resolution of 15,000. Protein identification was done with Byonic (Protein Metrics). A search was performed against the dog proteome (UP000002254_9615) with the addition of the human B3GNT2, B4GALT1, and ST6GAL1 sequences. The search was performed with specific digestion C-terminal of R/K, allowing 3 missed cleavages, using precursor and fragment mass tolerances of 12 and 24 ppm, respectively. Carbamidomethylation of cysteine was set as a fixed modification and oxidation of the methionine or tryptophan as a variable modification. Peptides unique for the human B3GNT2, B4GALT1, and ST6GAL1 were manually selected and the MS1 peak areas were integrated with Skyline and normalized against the combined MS1 signals for identified peptides of tubulin-β (E2RFJ7). The peptide library for Skyline was built by repeating the search with a focused database containing only the human B3GNT2, B4GALT1, and ST6GAL1 and tubulin-β sequences. The MS proteomic data have been deposited to the ProteomeXchange Consortium via the PRIDE (Perez-Riverol et al. 2022) partner repository with the data set identifier PXD037175.

Expression and purification of trimeric HA for binding studies

Recombinant trimeric IAV HA ectodomain proteins were cloned into the pCD5 expression vector as described previously (Zeng et al. 2008; de Vries et al. 2010), in frame with a GCN4 trimerization motif (KQIEDKIEEIESKQKKIENEIARIKK), a superfolder GFP (Nemanichvili et al. 2019) or mOrange2 (Shaner et al. 2008) and the Twin-Strep-tag (WSHPQFEKGGGSGGGSWSHPQFEK; IBA, Germany). An example of such a plasmid is Addgene plasmid #182546 (Broszeit et al. 2019), which contains the codon optimized HA sequence (synthesized by GenScript) of A/Vietnam/1203/2004 H5. The codon optimized genes of the other HAs (Table SXIII) were cloned into the plasmid using the restriction sites NheI and PacI. The trimeric HAs were expressed in HEK293S GnTI(−) cells with polyethyleneimine I (PEI) in a 1:8 ratio (μg DNA:μg PEI) for the HAs as previously described (de Vries et al. 2010), whereas a 1:12 ratio was used for the NTD of the guinea fowl CoV. The transfection mix was replaced after 6 h by 293 SFM II suspension medium (Invitrogen, 11686029), supplemented with sodium bicarbonate (3.7 g/L), Primatone RL-UF (3.0 g/L, Kerry, NY, USA), glucose (2.0 g/L), glutaMAX (1%, Gibco), valproic acid (0.4 g/L), and DMSO (1.5%). Culture supernatants were harvested 5 days post-transfection and purified with sepharose strep-tactin beads (IBA Life Sciences, Germany) according to the manufacturer's instructions.

Flow cytometry studies

Cells were harvested using TrypLE Express Enzyme as described above. After the removal of the supernatant, cells were resuspended in PBS supplemented with 1% FCS (S7524, Sigma) and 2 mM EDTA and kept at 4°C until the plate was measured in the flow cytometer. For experiments with α2–3,6,8,9 neuraminidase A (#P0722, New England Biolabs), neuraminidase (NA) was used 1:200 with 1,000,000 cells per ml in GlycoBuffer 1 (5 mM $CaCl_2$, 50 mM sodium acetate, in MQ water, at pH 5.5) for 16 h at 37°C on a shaking platform in the dark, before incubation with the lectin/HA mixes. In a round-bottom 96-wells plate (353910, Falcon), 150,000 cells were used. Per well, 100 μl of PBS supplemented with 1 μg of HA or biotinylated lectin (SNA (B1305), LEL (B1175), ECA (B1145), all from Vector Laboratories) was used, to achieve a final concentration of 10 μg/ml. HAs were precomplexed (on ice, 20 min) with 1.3 μg monoclonal antibody detecting the Twin-Strep-tag and 0.325 μg goat anti-human Alexa Fluor 488 (A11013, Invitrogen). Biotinylated lectins were precomplexed (on ice, 20 min) with 0.2 μg streptavidin Alexa Fluor 488 (S32354, Invitrogen). For titration experiments, different amounts of HA, lectin, precomplexing antibodies, or streptavidin were used. Furthermore, eBioscience Fixable Viability Dye eFluor 780 (65-0865, Thermo Fisher Scientific) was diluted 1:2,000 in the same mixture. Cells were incubated with the HA/lectin mix for 30 min at 4°C in the dark. Cells were washed once with PBS supplemented with 1% FCS and 2 mM EDTA, after which the cells were fixed with 100 μl of 1% paraformaldehyde in PBS for 10 min. Afterward, cells were washed once using PBS supplemented with 1% FCS and 2 mM EDTA, after which they were resuspended in 100 μl of the same buffer. Flow cytometry was performed using the BD FACSCanto II (BD Biosciences) using appropriate laser voltages. Data were analyzed using FlowLogic (Inivai Technologies) and gated as described in

Fig. 2a to consecutively select cells, single cells, and cells that are not dead. Mean fluorescence values of triplicates were averaged and standard deviations were calculated. Curves for titration experiments were smoothed using the standard settings.

Identification of N-glycans on cells by MS

Cell lysates of WT and B3GNT2/B4GALT1 knock-in MDCK and hCK cells were obtained as described above. The total protein concentration in the cell lysates was determined using a BCA assay. The glycans in 400 μg of total protein were released by PNGaseF treatment. Proteins were first denatured in DTT/SDS (40 mM DTT, 0.5% v/v SDS) for 8 min at 95°C, after which they were cooled on ice. Subsequently, NP-40 (1% v/v) and GlycoBuffer G7 (50 mM sodium phosphate at pH 7.5) were added, together with 30 μg of PNGaseF. The samples were incubated in a shaking incubator overnight at 37°C. Samples were centrifuged (4,700 rcf, 3 min) to remove potential precipitate, after which they were loaded on separate C18 SPE cartridges (Avantor 7020-02 BAKERBOND SPE Octadecyl), which were beforehand conditioned with 1 ml acetonitrile (MeCN) and 1 ml MQ water. The flow-through was collected and the remaining glycans were eluted from the C18 cartridges with 1 ml of 5% MeCN and 0.05% trifluoroacetic acid (TFA) in MQ water. The MeCN and TFA in both samples were evaporated under a stream of nitrogen gas. Flow through and elution fractions were diluted into 500 μl MQ water and combined, after which PGC SPE cartridges (Thermo Scientific HyperSep Hypercarb SPE cartridges) were used to further purify the samples according to procedures adapted from (Packer et al. 1998). The PGC SPE cartridges were conditioned with 1 ml MeCN and 1 ml MQ water, after which the samples were loaded on the cartridges. The cartridges were washed with 1 ml 0.05% TFA in MQ water and 1 ml 5% MeCN with 0.05% TFA in MQ water. Samples were eluted with 50% MeCN and 0.1% TFA in MQ water and evaporated under a stream of nitrogen gas. The dried glycans were dissolved in 30 μl MQ water and 6 μl pure glacial acetic acid and labeled using 5 μl procainamide (105 mg/ml procainamide HCl in DMSO) and 5 μl 2-picoline borane (107 mg/ml 2-Methylpyridine borane complex in DMSO; Ruhaak et al. 2010; Keser et al. 2018). The solution was vortexed thoroughly and incubated for 2 h at 65°C, after which the samples were evaporated using the vacuum concentrator. The sample was dissolved in 300 μl MQ water and vortexed until the pellets were dissolved, after which 5 μl 25% (w/v) ammonia was added per sample to ensure a pH above 10. To remove the unused procainamide from the reaction mixture, liquid–liquid extraction with 500 μl dichloromethane was performed 3 times, with centrifuge steps of 4,700 rcf for 3 min in between. The dichloromethane was removed and residual dichloromethane in the aqueous layer was evaporated under a stream of nitrogen gas. The samples were dissolved in a total of 1 ml MQ water after which they were loaded onto PGC SPE cartridges (conditioned with 2 ml MeCN and 2 ml MQ water). The cartridges were washed with 2 ml MQ water and the glycans were eluted using 50% MeCN with 0.1% TFA in MQ water, after which the MeCN and TFA were evaporated under a stream of nitrogen gas, followed by lyophilization.

Before HILIC-IMS-QTOF analysis, the lyophilized samples were reconstituted in 15 μl 70% MeCN in MQ water and centrifuged. The injected volume was 10 μl. The HILIC-IMS-QTOF system was an Agilent 1260 Infinity LC coupled to a 6560 IM-QTOF mass spectrometer (Agilent Technologies, Santa Clara, USA). For HILIC separation, a SeQuant ZIC-cHILIC column (3 μm, 100 Å; 150 × 2.1 mm) was used with a matching guard column (20 × 2.1 mm). The temperature of the column compartment was set at 40°C. The mobile phase was composed of eluent A: 10 mM ammonium formate with 10 mM FA in MQ water, and eluent B: LC–MS grade MeCN. The initial eluent composition was 30% A at a flow rate of 0.2 ml/min, followed by a linear gradient to 50% A from 0 to 20 min. 50% A was held isocratically until 25 min. To re-establish initial conditions, the column was flushed with at least 10 column volumes of 30% A.

The IMS-QTOF was set to positive ion mode with a capillary voltage of 3,500 V, nozzle voltage of 2,000 V, and a fragmentor voltage of 360 V. The drying gas temperature was 300°C with a flow rate of 8 l/min and the sheath gas temperature was 300°C at 11 l/min. The nebulizer pressure was set at 40 psi. The ion mobility settings were set as follows: 18 IM transients per frame, an IM trap fill time of 3,900 μs and a release time of 250 μs, the drift tube voltage was 1,400 V, and the multiplexing pulsing sequence length was 4 bits.

IM-MS data were calibrated to reference signals of *m/z* 121.050873 and 922.009798 using the IM-MS reprocessor utility of the Agilent Masshunter software. The mass-calibrated data was then demultiplexed using the PNNL preprocessor software using a 5-point moving average smoothing and interpolation of 3 drift bins. To find potential glycan hits in the processed data, the "find features" (IMFE) option of the Agilent IM-MS browser was used with the following criteria: "Glycans" isotope model, limited charge state to 5 and an ion intensity above 500. The found features were filtered by *m/z* range of 300–3,200 and an abundance of over 500 (a.u.) where abundance for a feature was defined as "max ion volume" (the peak area of the most abundant ion for that feature).

After exporting the list of filtered features, glycans with a mass below 1,129 Da (the mass of an *N*-glycan core) were removed. The ExPASy GlycoMod tool (Cooper et al. 2001) was used to search for glycan structures (monoisotopic mass values, 5 ppm mass tolerance, neutral, derivatized N-linked oligosaccharides, procainamide (mass 235.168462) as reducing terminal derivative, looking for underivatized monosaccharide residues (Hexose, HexNAc, Deoxyhexose, and NeuAc). Although we initially also screened for NeuGc, it did not provide plausible glycan composition hits. Instead, most possible NeuGc hits were isobaric Deoxyhexose + NeuGc = Hexose + NeuAc compositions, where the Hexose + NeuAc composition was deemed more realistic. Indeed, commonly observed NeuGcLacNAc (673.2298 *m/z*) in-source oxonium fragments were absent, whereas NeuAcLacNAc (657.2298 *m/z*) was found in high abundance. This is further supported by our previous work in which we showed that NeuGc is absent on MDCK cells (Broszeit et al. 2019). Thus, we removed NeuGc from the analysis to simplify the further processing of the data. For features with multiple potential monosaccharide combinations, the most realistic glycan in the biological context was chosen. The abundance of glycan features with the same mass, composition, and a maximum difference of 0.1 min in the retention time were combined as one isomer. Full glycan composition feature lists for the different cell lines are presented in Tables SII–SIX.

Table 1. Details of IAVs used in the experiment shown in Fig. 5a–c. These viruses include 1 older H3N2 virus from 2003, 1 H1N1 virus, and 2 influenza B viruses. The viruses were passaged in MDCK, MDCK-SIAT1 (Matrosovich et al. 2003), and/or hCK cells.

Virus	Virus details	Passage history
A/Netherlands/1797/2017	Subtype H3N2, clade 3C.2a1	SIAT2hCK2
A/Netherlands/371/2019	Subtype H3N2, clade 3C.2a1	SIAT2MDCK1hCK1
A/Netherlands/10009/2019	Subtype H3N2, clade 3C.2a1b	SIAT1hCK3
A/Netherlands/314/2019	Subtype H3N2, clade 3C.2a1b	SIAT2hCK2
A/Netherlands/384/2017	Subtype H3N2, clade 3C.3a	SIAT2hCK4
A/Netherlands/10006/2019	Subtype H3N2, clade 3C.3a	SIAT1hCK3
A/Netherlands/3466/2017	Subtype H3N2, clade 3C.2a2	SIAT2hCK2
A/Netherlands/10616/2019	Subtype H3N2, clade 3C.2a2	SIAT1hCK2
A/Netherlands/213/2003	Subtype H3N2	MDCK2
A/Netherlands/121/2020	Subtype H1N1	hCK2
B/Croatia/7789/2019	Lineage Victoria	MDCKxMDCK3
B/Netherlands/461/2019	Lineage Yamagata	SIAT5hCK1

Analysis of the number of LacNAc repeating units was performed on the complex and hybrid *N*-glycans with at least 1 LacNAc repeating unit. A glycan with 1 LacNAc repeating unit was defined as a glycan with 4 hexoses and a minimum of 3 HexNAcs or 3 HexNAcs and at least 4 hexoses. A glycan with 2 LacNAc repeating units was defined as a glycan with 5 hexoses and a minimum of 4 HexNAcs or 4 HexNAcs and at least 5 hexoses. This pattern was continued for the higher numbers of LacNAc repeating units. The total absolute abundance of all selected glycans was added up, after which the relative abundance of a given number of LacNAc repeating units was calculated from this total. Additionally, the percentage of these glycans with at least 1 Sia was calculated.

Chromatograms of the *N*-glycans with 2–7 LacNAc repeating units, calculated as described above, from hCK WT and hCK-B3GNT2 cells were constructed using Agilent's Masshunter Qualitative Analysis 10.0 software (Fig. 3a). The shown chromatograms are the summed extracted-ion-count (EIC) for the 10 most abundant glycan features per LacNAc repeating unit group. The EIC for a glycan was set as the observed *m/z* value with a symmetrical 10 ppm expansion. Different ionization states of the same glycan that were found as a separate feature by the feature-finding software were also included in the summed EIC chromatogram.

The MS/MS experiments were performed on a Thermo Scientific Exploris 480 connected to a Thermo Scientific Ultimate 3000 UPLC system. Solvent A consisted of 0.1% FA, solvent B of 0.1% FA in 80% acetonitrile. A 50 cm, 75 um ID, 2.4 um Reprosil column was used with a 60 min gradient of 2% B at 0–1 min, 44% B at 39 min, 55% B at 44 min, 99% B at 45–50 min, 2% B at 50–60 min. After an initial MS scan, and MS/MS scan, was triggered for ions with an intensity of more than 2e5 and a charge state from 2+ to 8+. The MS/MS scan used HCD at 15% NCE. All scans were performed with the instrument in peptide application mode.

Proteowizard MSconvert (version 3.0.21328-404bcf1) was used to convert Thermo raw files to MGF format using MGF as output format, 64-bit binary encoding precision and with the following options selected: write idex, zlib compression, and TPP compatibility. No filters were used when converting raw files to MGF format. To search MGF files for spectra containing glycan oxonium ions an internally developed tool named Peaksuite (v1.10.1) was used with an ion delta of 20 ppm, noise filter of 0%, and using a list of oxonium *m/z* values as mass targets (Table SX). Scans without any detected peaks were removed. Python 3.2.2 was used for data curation based on precursor *m/z* (10 ppm), retention time (17–24 min), and intensities of oxonium ions that originated from the glycan core (*m/z* 441.2707, 587.3286, 644.3501, 790.4080, 806.4029, and 952.4608). The sum intensity threshold of the core oxonium ions was set to 1e4. Python 3.2.2. was also used for calculating the relative intensities of oxonium ions normalized versus the sum intensities of the core oxonium ions.

Sugar nucleotide analysis

Cells were grown to 60–70% confluency in a 6-wells plate, after which the medium was removed and the cells were washed twice with wash buffer (75 mM ammonium carbonate in MQ water, pH 7.4 (corrected with glacial acetic acid), at 4°C). The cells were then treated with 700 μl of extraction buffer (40% acetonitrile, 40% methanol, 20% MQ water, at 4°C) per well for 2 min, after which the supernatant was transferred to a vial. This extraction step is repeated for 3 min, after which the 2 extracts were pooled and centrifuged at 18,000 rcf for 3 min. The supernatant was taken and dried in the vacuum concentrator. Samples were frozen at −80°C until analysis using an ion-pair UHPLC-QqQ 1290-6490 Agilent mass spectrometer by Glycomscan BV (Oss, The Netherlands; van Scherpenzeel et al. 2022).

Virus titration on B3GNT2/B4GALT1 knock-in MDCK and hCK cells

Virus titers in the virus stocks in Table 1 were determined using end-point titration in MDCK cells and inoculated cell cultures were tested for agglutination activity using turkey red blood cells as an indicator of virus replication in the cells. For recent (2017–2019) H3N2 viruses, no binding to erythrocytes was observed and therefore virus titers were determined using a nucleoprotein (NP) staining. The NP staining was performed on the inoculated cells that were fixed with acetone for at least 20 min at −20°C. Primary mouse anti-NP antibody (HB65, 2 mg/ml) was diluted 1:3,000 and the secondary goat anti-mouse IgG HRP antibody (A16702, 1 mg/ml, Thermo Fisher Scientific) was used at a dilution of 1:30,000, after which 50 μl per well was used for both solutions. True Blue substrate (KPL) was then added to visualize positive wells using an ImmunoSpot Analyzer (CTL Europe, Bonn, Germany). Based on the negative control values and the highest positive values per plate, the cut-off for positivity was determined. Infectious titers were calculated from 5 replicates using the Spearman–Kärber method (Kärber 1931).

Table 2. Details of H3N2 IAVs used in the experiment shown in Fig. 5d. The exact virus is indicated as well as the clade and HA mutations if applicable. Previous attempts of isolating these viruses in hCK cells were either unsuccessful (−) or successful (+).

Number	Virus	Clade (+ HA mutations)	Cultured previously
1	A/Netherlands/3425/2017	3C.2a	−
2	A/Netherlands/2362/2018	3C.2a1b	−
3	A/Netherlands/2380/2018	3C.2a1b	−
4	A/Netherlands/010/2019	3C.2a1b	−
5	A/Netherlands/173/2019	3C.2a1b	−
6	A/Netherlands/1268/2019	3C.2a4	−
7	A/Netherlands/1735/2019	3C.2a1b + T135K	−
8	A/Netherlands/1747/2019	3C.2a1b + T135K	−
9	A/Netherlands/1439/2019	3C.2a1b	+
10	A/Netherlands/1734/2019	3C.2a1b + T135K	+
11	A/Netherlands/054/2020	3C.2a1b + T131K	+
12	A/Netherlands/008/2021	3C.2a1b.2a2	+

Inoculation of hCK and hCK-B3GNT2 cells with influenza viruses

To evaluate whether IAVs that could not be isolated previously in hCK cells would replicate in hCK-B3GNT2 cells, hCK and hCK-B3GNT2 cells were seeded at a density of 20,000 cells per well in 96-wells plates at 24 h before inoculation. The original patient materials (100 μl), which are influenza virus positive swabs collected as part of the Dutch influenza virus surveillance program, (details of viruses in Table 2) were diluted in 700 μl infection medium (EMEM (Cambrex, Heerhugowaard, The Netherlands) supplemented with 100 U/ml penicillin, 100 μg/ml streptomycin, 2 mM glutamine, 1.5 mg/ml sodium bicarbonate (Cambrex), 10 mM Hepes (Cambrex), nonessential amino acids (MP Biomedicals) and 20 μg/ml trypsin (Cambrex)), after which a 2-fold dilution series was made. After 3 days, the presence or absence of cytopathic effects in each well was scored and the mean (n = 3) of the number of infected wells was calculated.

Author contributions

Cindy M. Spruit (Conceptualization-Equal, Data curation-Equal, Formal analysis-Lead, Investigation-Equal, Methodology-Equal, Visualization-Lead, Writing—original draft-Lead), Igor R. Sweet (Formal analysis-Equal, Investigation-Equal, Methodology-Equal, Software-Equal), Joshua C.L. Maliepaard (Formal analysis-Equal, Investigation-Equal, Methodology-Equal, Software-Equal), Theo Bestebroer (Formal analysis-Equal, Investigation-Equal), Pascal Lexmond (Formal analysis-Equal, Investigation-Equal), Boning Qiu (Methodology-Equal), Mirjam J.A. Damen (Investigation-Equal), Ron A.M. Fouchier (Funding acquisition-Equal, Writing—review & editing-Equal), Karli R. Reiding (Formal analysis-Equal, Investigation-Equal, Methodology-Equal), Joost Snijder (Formal analysis-Equal, Funding acquisition-Equal, Investigation-Equal, Methodology-Equal, Writing—original draft-Supporting), Sander Herfst (Formal analysis-Equal, Funding acquisition-Equal, Investigation-Equal, Writing—review & editing-Equal), Geert-Jan Boons (Funding acquisition-Equal, Writing—review & editing-Lead), **and** Robert P. de Vries (Conceptualization-Lead, Data curation-Equal, Funding acquisition-Lead, Resources-Lead, Supervision-Lead, Visualization-Equal, Writing—review & editing-Lead)

Abbreviations

IAV, influenza A virus; LacNAc, N-acetyllactosamine; HA, hemagglutinin; Sia, sialic acid; MDCK, Madin-Darby Canine Kidney; hCK, "humanized" MDCK; B3GNT2, β-1,3-N-acetylglucosaminyltransferase; B4GALT1, β-1,4-galactosyltransferase 1; SNA, *Sambucus nigra* agglutinin; LEL, *Lycopersicon esculentum* lectin; WT, wild-type, ECA, *Erythrina cristagalli* lectin; Gf-CoV-2014 NTD, N-terminal domain of γCoV/AvCoV/guinea fowl/France/14032/2014; H5VN, A/Vietnam/1203/2004 H5N1; PR8, A/Puerto-Rico/8/1934 H1N1; B3, B3GNT2; B4, B4GALT1; TCEP, tris(2-carboxyethyl)phosphine; CAA, chloroacetamide; SDC, sodium deoxycholate; FA, formic acid; SPE, solid-phase extraction; MS, mass spectrometry, PEI, polyethyleneimine; NA, neuraminidase; MeCN, acetonitrile; TFA, trifluoroacetic acid; EIC, extracted-ion-count; NP, nucleoprotein; NeuGc, *N*-glycolylneuraminic acid; NeuAc, *N*-acetylneuraminic acid; KDN, 2-keto-3-deoxynonic acid; HCD, higher-energy collisional dissociation; NCE, normalized collision energy.

Acknowledgments

We thank Professor Yoshihiro Kawaoka for providing the hCK cells. We would like to thank Frederik Broszeit for producing the glycans that are used in the glycan microarray in Fig. S2. Balthasar Heesters is thanked for his advice on the flow cytometry experiments and analysis. We thank Gerlof Bosman for the production of PNGaseF. Monique van Scherpenzeel is thanked for the sugar nucleotide analysis. We also thank Roosmarijn van der Woude and Alinda Berends for their technical assistance.

Supplementary material

Supplementary material is available at *Glycobiology Journal* online.

Funding

The European Commission (ERC Starting Grant 802780 to RPdV); the Royal Dutch Academy of Sciences (Beijerinck Premium to RPdV); the Dutch Research Council (NWO Gravitation 2013 BOO, Institute for Chemical Immunology (ICI; 024.002.009) to JS); NIAID/NIH Centers of Excellence (Influenza Research and Response contract 75N93021C00014 to RAMF and SH).

Conflict of interest statement. None declared.

Data availability

The mass spectrometry proteomic data (for the quantification of B3GNT2, B4GALT1, and ST6GAL1 proteins) have been deposited to the ProteomeXchange Consortium via the PRIDE (Perez-Riverol et al. 2022) partner repository with the data set identifier PXD037175. The released *N*-glycan raw data (for the glycomic analyses of the cell lines) have been deposited to the GlycoPOST repository (Watanabe et al. 2021) under identifier GPST000345.

References

Achdout H, Meningher T, Hirsh S, Glasner A, Bar-On Y, Gur C, Porgador A, Mendelson M, Mandelboim M, Mandelboim O. Killing of avian and swine influenza virus by natural killer cells. *J Virol*. 2010:**84**(8):3993–4001.

Allen JD, Ross TM. H3N2 influenza viruses in humans: viral mechanisms, evolution, and evaluation. *Hum Vaccin Immunother*. 2018:**14**(8):1840–1847.

Arnon TI, Achdout H, Lieberman N, Gazit R, Gonen-Gross T, Katz G, Bar-Ilan A, Bloushtain N, Lev M, Joseph A, et al. The mechanisms controlling the recognition of tumor- and virus-infected cells by NKp46. *Blood*. 2004:**103**(2):664–672.

Asaoka N, Tanaka Y, Sakai T, Fujii Y, Ohuchi R, Ohuchi M. Low growth ability of recent influenza clinical isolates in MDCK cells is due to their low receptor binding affinities. *Microbes Infect*. 2006:**8**(2):511–519.

Bouwman KM, Delpont M, Broszeit F, Berger R, Weerts E, Lucas MN, Delverdier M, Belkasmi S, Papanikolaou A, Boons GJ, et al. Guinea fowl coronavirus diversity has phenotypic consequences for glycan and tissue binding. *J Virol*. 2019:**93**(10):00067-19. https://doi.org/10.1128/JVI.00067-19.

Broszeit F, Tzarum N, Zhu X, Nemanichvili N, Eggink D, Leenders T, Li Z, Liu L, Wolfert MA, Papanikolaou A, et al. N-glycolylneuraminic acid as a receptor for influenza A viruses. *Cell Rep*. 2019:**27**(11):3284–3294.e6.

Broszeit F, van Beek RJ, Unione L, Bestebroer TM, Chapla D, Yang JY, Moremen KW, Herfst S, Fouchier RAM, de Vries RP, et al. Glycan remodeled erythrocytes facilitate antigenic characterization of recent A/H3N2 influenza viruses. *Nat Commun*. 2021:**12**(1):5449.

Byrd-Leotis L, Gao C, Jia N, Mehta AY, Trost J, Cummings SF, Heimburg-Molinaro J, Cummings RD, Steinhauer DA. Antigenic pressure on H3N2 influenza virus drift strains imposes constraints on binding to sialylated receptors but not phosphorylated glycans. *J Virol*. 2019a:**93**(22):01178-19.

Byrd-Leotis L, Jia N, Dutta S, Trost JF, Gao C, Cummings SF, Braulke T, Muller-Loennies S, Heimburg-Molinaro J, Steinhauer DA, et al. Influenza binds phosphorylated glycans from human lung. *Sci Adv*. 2019b:**5**(2):eaav2554.

Byrd-Leotis L, Jia N, Matsumoto Y, Lu D, Kawaoka Y, Steinhauer DA, Cummings RD. Sialylated and sulfated N-Glycans in MDCK and engineered MDCK cells for influenza virus studies. *Sci Rep*. 2022:**12**(1):12757.

Canales A, Sastre J, Orduña JM, Spruit CM, Pérez-Castells J, Domínguez G, Bouwman KM, van der Woude R, Cañada FJ, Nycholat CM, et al. Revealing the specificity of human H1 influenza A viruses to complex N-Glycans. *JACS Au*. 2023:**3**(3):868–878.

Canals I, Ginisty A, Quist E, Timmerman R, Fritze J, Miskinyte G, Monni E, Hansen MG, Hidalgo I, Bryder D, et al. Rapid and efficient induction of functional astrocytes from human pluripotent stem cells. *Nat Methods*. 2018:**15**(9):693–696.

Chambers BS, Li Y, Hodinka RL, Hensley SE. Recent H3N2 influenza virus clinical isolates rapidly acquire hemagglutinin or neuraminidase mutations when propagated for antigenic analyses. *J Virol*. 2014:**88**(18):10986–10989.

Chan CM, Chu H, Zhang AJ, Leung LH, Sze KH, Kao RY, Chik KK, To KK, Chan JF, Chen H, et al. Hemagglutinin of influenza A virus binds specifically to cell surface nucleolin and plays a role in virus internalization. *Virology*. 2016:**494**:78–88.

Chandrasekaran A, Srinivasan A, Raman R, Viswanathan K, Raguram S, Tumpey TM, Sasisekharan V, Sasisekharan R. Glycan topology determines human adaptation of avian H5N1 virus hemagglutinin. *Nat Biotechnol*. 2008:**26**(1):107–113.

Chu VC, Whittaker GR. Influenza virus entry and infection require host cell N-linked glycoprotein. *Proc Natl Acad Sci U S A*. 2004:**101**(52):18153–18158.

Cole NB, Smith CL, Sciaky N, Terasaki M, Edidin M, Lippincott-Schwartz J. Diffusional mobility of Golgi proteins in membranes of living cells. *Science*. 1996:**273**(5276):797–801.

Cooper CA, Gasteiger E, Packer NH. GlycoMod - a software tool for determining glycosylation compositions from mass spectrometric data. *Proteomics*. 2001:**1**(2):340–349.

Dull T, Zufferey R, Kelly M, Mandel RJ, Nguyen M, Trono D, Naldini L. A third-generation lentivirus vector with a conditional packaging system. *J Virol*. 1998:**72**(11):8463–8471.

Eierhoff T, Hrincius ER, Rescher U, Ludwig S, Ehrhardt C. The epidermal growth factor receptor (EGFR) promotes uptake of influenza A viruses (IAV) into host cells. *PLoS Pathog*. 2010:**6**(9):e1001099.

Fujioka Y, Nishide S, Ose T, Suzuki T, Kato I, Fukuhara H, Fujioka M, Horiuchi K, Satoh AO, Nepal P, et al. A sialylated voltage-dependent Ca(2+) channel binds hemagglutinin and mediates influenza A virus entry into mammalian cells. *Cell Host Microbe*. 2018:**23**(6):809–818.e5.

Gambaryan A, Yamnikova S, Lvov D, Tuzikov A, Chinarev A, Pazynina G, Webster R, Matrosovich M, Bovin N. Receptor specificity of influenza viruses from birds and mammals: new data on involvement of the inner fragments of the carbohydrate chain. *Virology*. 2005:**334**(2):276–283.

Gulati S, Smith DF, Cummings RD, Couch RB, Griesemer SB, St George K, Webster RG, Air GM. Human H3N2 influenza viruses isolated from 1968 to 2012 show varying preference for receptor substructures with no apparent consequences for disease or spread. *PLoS One*. 2013:**8**(6):e66325.

Hatakeyama S, Sakai-Tagawa Y, Kiso M, Goto H, Kawakami C, Mitamura K, Sugaya N, Suzuki Y, Kawaoka Y. Enhanced expression of an alpha2,6-linked sialic acid on MDCK cells improves isolation of human influenza viruses and evaluation of their sensitivity to a neuraminidase inhibitor. *J Clin Microbiol*. 2005:**43**(8):4139–4146.

Ho JW, Hershkovitz O, Peiris M, Zilka A, Bar-Ilan A, Nal B, Chu K, Kudelko M, Kam YW, Achdout H, et al. H5-type influenza virus hemagglutinin is functionally recognized by the natural killer-activating receptor NKp44. *J Virol*. 2008:**82**(4):2028–2032.

Hossler P, Mulukutla BC, Hu WS. Systems analysis of N-glycan processing in mammalian cells. *PLoS One*. 2007:**2**(8):e713.

Jester BJ, Uyeki TM, Jernigan DB. Fifty years of influenza A(H3N2) following the pandemic of 1968. *Am J Public Health*. 2020:**110**(5):669–676.

Jia N, Barclay WS, Roberts K, Yen HL, Chan RW, Lam AK, Air G, Peiris JS, Dell A, Nicholls JM, et al. Glycomic characterization of respiratory tract tissues of ferrets: implications for its use in influenza virus infection studies. *J Biol Chem*. 2014:**289**(41):28489–28504.

Jia N, Byrd-Leotis L, Matsumoto Y, Gao C, Wein AN, Lobby JL, Kohlmeier JE, Steinhauer DA, Cummings RD. The human lung glycome reveals novel glycan ligands for influenza a virus. *Sci Rep*. 2020:**10**(1):5320.

Karakus U, Pohl MO, Stertz S. Breaking the convention: sialoglycan variants, coreceptors, and alternative receptors for influenza a virus entry. *J Virol*. 2020:**94**(4):01357-19. https://doi.org/10.1128/JVI.01357-19.

Kärber G. Beitrag zur kollektiven Behandlung pharmakologischer Reihenversuche. *Naunyn Schmiedebergs Arch Exp Pathol Pharmakol*. 1931:**162**(4):480–483.

Keser T, Pavic T, Lauc G, Gornik O. Comparison of 2-aminobenzamide, procainamide and RapiFluor-MS as derivatizing agents for high-throughput HILIC-UPLC-FLR-MS N-glycan analysis. *Front Chem*. 2018:**6**:324.

Kumari K, Gulati S, Smith DF, Gulati U, Cummings RD, Air GM. Receptor binding specificity of recent human H3N2 influenza viruses. *Virol J*. 2007:**4**(1):42.

Lee HK, Tang JW, Kong DH, Loh TP, Chiang DK, Lam TT, Koay ES. Comparison of mutation patterns in full-genome A/H3N2 influenza sequences obtained directly from clinical samples and the same samples after a single MDCK passage. *PLoS One*. 2013:**8**(11):e79252.

Li T, Liu L, Wei N, Yang JY, Chapla DG, Moremen KW, Boons GJ. An automated platform for the enzyme-mediated assembly of complex oligosaccharides. *Nat Chem*. 2019:**11**(3):229–236.

Lin YP, Xiong X, Wharton SA, Martin SR, Coombs PJ, Vachieri SG, Christodoulou E, Walker PA, Liu J, Skehel JJ, et al. Evolution of the receptor binding properties of the influenza A(H3N2) hemagglutinin. *Proc Natl Acad Sci U S A*. 2012:**109**(52):21474–21479.

Lin Y, Wharton SA, Whittaker L, Dai M, Ermetal B, Lo J, Pontoriero A, Baumeister E, Daniels RS, McCauley JW. The characteristics and antigenic properties of recently emerged subclade 3C.3a and 3C.2a human influenza A(H3N2) viruses passaged in MDCK cells. *Influenza Other Respir Viruses*. 2017:**11**(3):263–274.

Liu L, Prudden AR, Capicciotti CJ, Bosman GP, Yang JY, Chapla DG, Moremen KW, Boons GJ. Streamlining the chemoenzymatic synthesis of complex N-glycans by a stop and go strategy. *Nat Chem*. 2019:**11**(2):161–169.

Liu M, Huang LZX, Smits AA, Bull C, Narimatsu Y, van Kuppeveld FJM, Clausen H, de Haan CAM, de Vries E. Human-type sialic acid receptors contribute to avian influenza A virus binding and entry by hetero-multivalent interactions. *Nat Commun*. 2022:**13**(1):4054.

Mandelboim O, Lieberman N, Lev M, Paul L, Arnon TI, Bushkin Y, Davis DM, Strominger JL, Yewdell JW, Porgador A. Recognition of haemagglutinins on virus-infected cells by NKp46 activates lysis by human NK cells. *Nature*. 2001:**409**(6823):1055–1060.

Mastrangeli R, Audino MC, Palinsky W, Broly H, Bierau H. The formidable challenge of controlling high mannose-type N-Glycans in therapeutic mAbs. *Trends Biotechnol*. 2020:**38**(10):1154–1168.

Matrosovich M, Matrosovich T, Carr J, Roberts NA, Klenk HD. Overexpression of the alpha-2,6-sialyltransferase in MDCK cells increases influenza virus sensitivity to neuraminidase inhibitors. *J Virol*. 2003:**77**(15):8418–8425.

Medeiros R, Escriou N, Naffakh N, Manuguerra JC, van der Werf S. Hemagglutinin residues of recent human A(H3N2) influenza viruses that contribute to the inability to agglutinate chicken erythrocytes. *Virology*. 2001:**289**(1):74–85.

Nemanichvili N, Tomris I, Turner HL, McBride R, Grant OC, van der Woude R, Aldosari MH, Pieters RJ, Woods RJ, Paulson JC, et al. Fluorescent trimeric hemagglutinins reveal multivalent receptor binding properties. *J Mol Biol*. 2019:**431**(4):842–856.

Nycholat CM, McBride R, Ekiert DC, Xu R, Rangarajan J, Peng W, Razi N, Gilbert M, Wakarchuk W, Wilson IA, et al. Recognition of sialylated poly-N-acetyllactosamine chains on N- and O-linked glycans by human and avian influenza A virus hemagglutinins. *Angew Chem Int Ed Engl*. 2012:**51**(20):4860–4863.

Oh DY, Barr IG, Mosse JA, Laurie KL. MDCK-SIAT1 cells show improved isolation rates for recent human influenza viruses compared to conventional MDCK cells. *J Clin Microbiol*. 2008:**46**(7):2189–2194.

Packer NH, Lawson MA, Jardine DR, Redmond JW. A general approach to desalting oligosaccharides released from glycoproteins. *Glycoconj J*. 1998:**15**(8):737–747.

Peck H, Laurie KL, Rockman S, Leung V, Lau H, Soppe S, Rynehart C, Baas C, Trusheim H, Barr IG. Enhanced isolation of influenza viruses in qualified cells improves the probability of well-matched vaccines. *NPJ Vaccines*. 2021:**6**(1):149.

Peng W, de Vries RP, Grant OC, Thompson AJ, McBride R, Tsogtbaatar B, Lee PS, Razi N, Wilson IA, Woods RJ, et al. Recent H3N2 viruses have evolved specificity for extended, branched human-type receptors, conferring potential for increased avidity. *Cell Host Microbe*. 2017:**21**(1):23–34.

Perez-Riverol Y, Bai J, Bandla C, Garcia-Seisdedos D, Hewapathirana S, Kamatchinathan S, Kundu DJ, Prakash A, Frericks-Zipper A, Eisenacher M, et al. The PRIDE database resources in 2022: a hub for mass spectrometry-based proteomics evidences. *Nucleic Acids Res*. 2022:**50**(D1):D543–D552.

Qiu B, de Vries RJ, Caiazzo M. Direct cell reprogramming of mouse fibroblasts into functional astrocytes using lentiviral overexpression of the transcription factors NFIA, NFIB, and SOX9. *Methods Mol Biol*. 2021:**2352**:31–43.

Ren WW, Jin ZC, Dong W, Kitajima T, Gao XD, Fujita M. Glycoengineering of HEK293 cells to produce high-mannose-type N-glycan structures. *J Biochem*. 2019:**166**(3):245–258.

Rimmelzwaan GF, Nieuwkoop NJ, de Mutsert G, Boon AC, Kuiken T, Fouchier RA, Osterhaus AD. Attachment of infectious influenza A viruses of various subtypes to live mammalian and avian cells as measured by flow cytometry. *Virus Res*. 2007:**129**(2):175–181.

Rogers GN, Paulson JC. Receptor determinants of human and animal influenza virus isolates: differences in receptor specificity of the H3 hemagglutinin based on species of origin. *Virology*. 1983:**127**(2):361–373.

Ruhaak LR, Steenvoorden E, Koeleman CA, Deelder AM, Wuhrer M. 2-picoline-borane: a non-toxic reducing agent for oligosaccharide labeling by reductive amination. *Proteomics*. 2010:**10**(12):2330–2336.

van Scherpenzeel M, Conte F, Bull C, Ashikov A, Hermans E, Willems A, van Tol W, Kragt E, Noga M, Moret EE, et al. Dynamic tracing of sugar metabolism reveals the mechanisms of action of synthetic sugar analogs. *Glycobiology*. 2022:**32**(3):239–250.

Shaner NC, Lin MZ, McKeown MR, Steinbach PA, Hazelwood KL, Davidson MW, Tsien RY. Improving the photostability of bright monomeric orange and red fluorescent proteins. *Nat Methods*. 2008:**5**(6):545–551.

Shibuya N, Goldstein IJ, Broekaert WF, Nsimba-Lubaki M, Peeters B, Peumans WJ. The elderberry (*Sambucus nigra* L.) bark lectin recognizes the Neu5Ac(alpha 2-6)Gal/GalNAc sequence. *J Biol Chem*. 1987:**262**(4):1596–1601.

Sieben C, Sezgin E, Eggeling C, Manley S. Influenza A viruses use multivalent sialic acid clusters for cell binding and receptor activation. *PLoS Pathog*. 2020:**16**(7):e1008656.

Spruit CM, Nemanichvili N, Okamatsu M, Takematsu H, Boons GJ, de Vries RP. N-glycolylneuraminic acid in animal models for human influenza A virus. *Viruses*. 2021:**13**(5):815.

Spruit CM, Zhu X, Tomris I, Ríos-Carrasco M, Han AX, Broszeit F, van der Woude R, Bouwman KM, Luu MMT, Matsuno K, et al. N-glycolylneuraminic acid binding of avian and equine H7 influenza A viruses. *J Virol*. 2022:**96**(5):e0212021.

Sriwilaijaroen N, Nakakita SI, Kondo S, Yagi H, Kato K, Murata T, Hiramatsu H, Kawahara T, Watanabe Y, Kanai Y, et al. N-glycan structures of human alveoli provide insight into influenza A virus infection and pathogenesis. *FEBS J*. 2018:**285**(9):1611–1634.

Stevens J, Blixt O, Glaser L, Taubenberger JK, Palese P, Paulson JC, Wilson IA. Glycan microarray analysis of the hemagglutinins from modern and pandemic influenza viruses reveals different receptor specificities. *J Mol Biol*. 2006:**355**(5):1143–1155.

Stevens J, Chen LM, Carney PJ, Garten R, Foust A, Le J, Pokorny BA, Manojkumar R, Silverman J, Devis R, et al. Receptor specificity of influenza A H3N2 viruses isolated in mammalian cells and embryonated chicken eggs. *J Virol*. 2010:**84**(16):8287–8299.

Sweeney JG, Liang J, Antonopoulos A, Giovannone N, Kang S, Mondala TS, Head SR, King SL, Tani Y, Brackett D, et al. Loss of GCNT2/I-branched glycans enhances melanoma growth and survival. *Nat Commun*. 2018:**9**(1):3368.

Takada K, Kawakami C, Fan S, Chiba S, Zhong G, Gu C, Shimizu K, Takasaki S, Sakai-Tagawa Y, Lopes TJS, et al. A humanized MDCK cell line for the efficient isolation and propagation of human influenza viruses. *Nat Microbiol*. 2019:**4**(8):1268–1273.

de Vries RP, de Vries E, Bosch BJ, de Groot RJ, Rottier PJ, de Haan CA. The influenza A virus hemagglutinin glycosylation state affects receptor-binding specificity. *Virology*. 2010:**403**(1):17–25.

Walther T, Karamanska R, Chan RW, Chan MC, Jia N, Air G, Hopton C, Wong MP, Dell A, Malik Peiris JS, et al. Glycomic analysis of human respiratory tract tissues and correlation with influenza virus infection. *PLoS Pathog*. 2013:**9**(3):e1003223.

Wang X, Xu Z, Tian Z, Zhang X, Xu D, Li Q, Zhang J, Wang T. The EF-1α promoter maintains high-level transgene expression from episomal vectors in transfected CHO-K1 cells. *J Cell Mol Med*. 2017:**21**(11):3044–3054.

Wang Q, Wang T, Yang S, Sha S, Wu WW, Chen Y, Paul JT, Shen RF, Cipollo JF, Betenbaugh MJ. Metabolic engineering challenges of extending N-glycan pathways in Chinese hamster ovary cells. *Metab Eng*. 2020:**61**:301–314.

Watanabe Y, Aoki-Kinoshita KF, Ishihama Y, Okuda S. GlycoPOST realizes FAIR principles for glycomics mass spectrometry data. *Nucleic Acids Res*. 2021:**49**(D1):D1523–D1528.

Watters KE, Fellmann C, Bai HB, Ren SM, Doudna JA. Systematic discovery of natural CRISPR-Cas12a inhibitors. *Science*. 2018:**362**(6411):236–239.

Yang H, Carney PJ, Chang JC, Guo Z, Villanueva JM, Stevens J. Structure and receptor binding preferences of recombinant human A(H3N2) virus hemagglutinins. *Virology*. 2015:**477**:18–31.

Zeng Q, Langereis MA, van Vliet AL, Huizinga EG, de Groot RJ. Structure of coronavirus hemagglutinin-esterase offers insight into corona and influenza virus evolution. *Proc Natl Acad Sci U S A*. 2008:**105**(26):9065–9069.